Cell Stem Cell

Contractile Forces Sustain and Polarize Hematopoiesis from Stem and Progenitor Cells

Cell Stem Cell, 21 November 2013

10.1016/j.stem.2013.10.009

Authors

Jae-Won Shin, Amnon Buxboim, Kyle R. Spinler, Joe Swift, David A. Christian, Christopher A. Hunter, Catherine Léon, Christian Gachet, P.C. Dave P. Dingal, Irena L. Ivanovska, Florian Rehfeldt, Joel Anne Chasis, Dennis E. Discher ✉ See Affiliations

Graphical Abstract

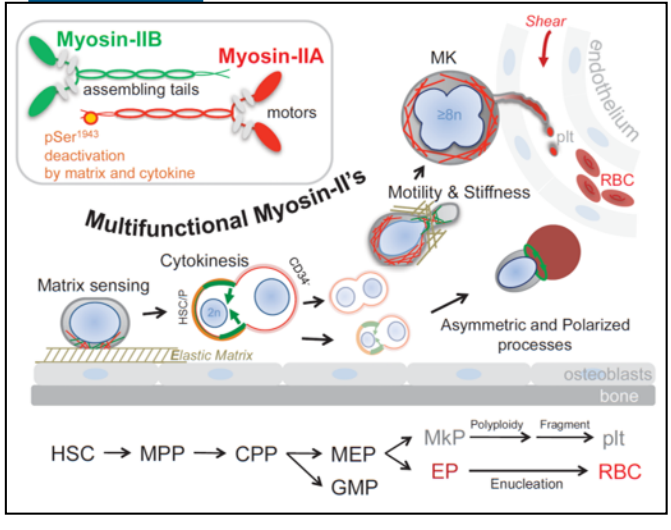

Highlights

- A and B isoforms of myosin-II switch in hematopoietic differentiation
- Polarizable myosin-IIB contributes to asymmetric division
- Niche-sensitive, essential myosin-IIA is increasingly activated in differentiation
- Inhibiting myosin-II enriches for long-term hematopoietic stem and progenitors

Summary

Self-renewal and differentiation of stem cells depend on asymmetric division and polarized motility processes that in other cell types are modulated by nonmuscle myosin-II (MII) forces and matrix mechanics. Here, mass spectrometry-calibrated intracellular flow cytometry of human hematopoiesis reveals MIIB to be a major isoform that is strongly polarized in hematopoietic stem cells and progenitors (HSC/Ps) and thereby downregulated in differentiated cells via asymmetric division. MIIA is constitutive and activated by dephosphorylation during cytokine-triggered differentiation of cells grown on stiff, endosteum-like matrix, but not soft, marrow-like matrix. In vivo, MIIB is required for generation of blood, while MIIA is required for sustained HSC/P engraftment. Reversible inhibition of both isoforms in culture with blebbistatin enriches for long-term hematopoietic multilineage reconstituting cells by 5-fold or more as assessed in vivo. Megakaryocytes also become more polyploid, producing 4-fold more platelets. MII is thus a multifunctional node in polarized division and niche sensing.

Please cite this article in press as: Shin et al., Contractile Forces Sustain and Polarize Hematopoiesis from Stem and Progenitor Cells, Cell Stem Cell (2014), http://dx.doi.org/10.1016/j.stem.2013.10.009

Cell Stem Cell
Article

Contractile Forces Sustain and Polarize Hematopoiesis from Stem and Progenitor Cells

Jae-Won Shin,[1,2] Amnon Buxboim,[1] Kyle R. Spinler,[1] Joe Swift,[1] David A. Christian,[3] Christopher A. Hunter,[3] Catherine Léon,[4] Christian Gachet,[4] P.C. Dave P. Dingal,[1] Irena L. Ivanovska,[1] Florian Rehfeldt,[1] Joel Anne Chasis,[5,6] and Dennis E. Discher[1,2,*]

[1]Biophysical Engineering Lab, University of Pennsylvania, Philadelphia, PA 19104, USA
[2]Cell and Molecular Biology and Pharmacology Graduate Groups, University of Pennsylvania, Philadelphia, PA 19104, USA
[3]Department of Pathobiology, School of Veterinary Medicine, University of Pennsylvania, Philadelphia, PA 19104, USA
[4]UMR S949, Inserm, Université de Strasbourg, Établissement Français du Sang, Strasbourg, 67000, France
[5]Life Sciences Division, University of California, Lawrence Berkeley National Laboratory, Berkeley, CA 94720, USA
[6]Division of Hematology/Oncology, University of California, San Francisco, San Francisco, CA 94143, USA
*Correspondence: discher@seas.upenn.edu
http://dx.doi.org/10.1016/j.stem.2013.10.009

SUMMARY

Self-renewal and differentiation of stem cells depend on asymmetric division and polarized motility processes that in other cell types are modulated by nonmuscle myosin-II (MII) forces and matrix mechanics. Here, mass spectrometry-calibrated intracellular flow cytometry of human hematopoiesis reveals MIIB to be a major isoform that is strongly polarized in hematopoietic stem cells and progenitors (HSC/Ps) and thereby downregulated in differentiated cells via asymmetric division. MIIA is constitutive and activated by dephosphorylation during cytokine-triggered differentiation of cells grown on stiff, endosteum-like matrix, but not soft, marrow-like matrix. In vivo, MIIB is required for generation of blood, while MIIA is required for sustained HSC/P engraftment. Reversible inhibition of both isoforms in culture with blebbistatin enriches for long-term hematopoietic multilineage reconstituting cells by 5-fold or more as assessed in vivo. Megakaryocytes also become more polyploid, producing 4-fold more platelets. MII is thus a multifunctional node in polarized division and niche sensing.

INTRODUCTION

Stem cells must be able to self-renew and also give rise to diverse cell types by asymmetric division in appropriate microenvironments (Knoblich, 2010). This differential segregation of cell fate determinants produces progenitors that expand symmetrically to generate tissue. Hematopoietic stem cells (HSCs, as a subset of $CD34^+$ cells) exemplify these key properties of stem cells in that they are often quiescent in niches of the bone marrow (BM), but they and/or their daughter cells polarize and divide asymmetrically in suitable niches to generate progenitors that further divide and specialize to terminally differentiated erythroid, megakaryocyte, and white cell lineages. A number of models for marrow and soluble signal regulation of HSC maintenance and differentiation have been described (Trumpp et al., 2010), but many physical aspects of hematopoiesis remain unclear. Many cell types apply forces to the matrix that they adhere to, and the flexibility of extracellular matrix is already known to modulate differentiation of marrow-derived mesenchymal stem cells (MSCs) (Engler et al., 2006) as well as the expansion of adult HSCs and progenitors (HSC/Ps) (Holst et al., 2010). In both of these latter studies, myosin-II (MII) inhibition revealed a key role for actomyosin forces in adhesion and sensing of matrix. However, cell contractile forces contribute to many processes in stem cell and progenitor maintenance and division with likely relationships to differentiation.

Cytokinesis is driven by nonmuscle MII in a cell's cortex, and the asymmetry of stem cell division in *C. elegans* is also established by MII (Ou et al., 2010). Differentiation in embryogenesis indeed requires active MII (Conti et al., 2004), and while inhibition of MII in adherent embryonic stem cells (ESCs) increases survival in culture by preserving intercellular contacts (Chen et al., 2010), inhibition can also lead to multinucleated cells (Canman et al., 2003). Actomyosin forces generally stabilize the plasma membrane with an active cortical tension or rigidity (Merkel et al., 2000), but these forces also drive cell rounding in cytokinesis (Sedzinski et al., 2011) and can change dramatically in differentiation (of MSCs) (Engler et al., 2006). Indeed, while it has been known for many years that as granulocytes differentiate they become soft to better traffic from marrow through the endothelial barrier and into the circulation (Lichtman, 1970), any MII changes in such cells leaving the marrow or in other hematopoietic cells is currently unknown.

Mammals express three isoforms of MII: A (*MYH9*), B (*MYH10*), and C (*MYH14*), and each is regulated transcriptionally as well as posttranslationally. MIIA is found in most tissues (Ma et al., 2010) including blood (Maupin et al., 1994) and is essential to embryonic differentiation (Conti et al., 2004). MIIB is particularly enriched in brain and cardiac tissues, and it is often polarized to the rear of migrating cells (Vicente-Manzanares et al., 2008; Raab et al., 2012). Recent studies have revealed roles for MIIB in hematopoiesis, specifically in megakaryocyte (MK) differentiation (Lordier et al., 2012) and in the asymmetric process of erythroid enucleation (Ubukawa et al., 2012). MIIB myofilaments are known to attach more strongly to and detach

Please cite this article in press as: Shin et al., Contractile Forces Sustain and Polarize Hematopoiesis from Stem and Progenitor Cells, Cell Stem Cell (2014), http://dx.doi.org/10.1016/j.stem.2013.10.009

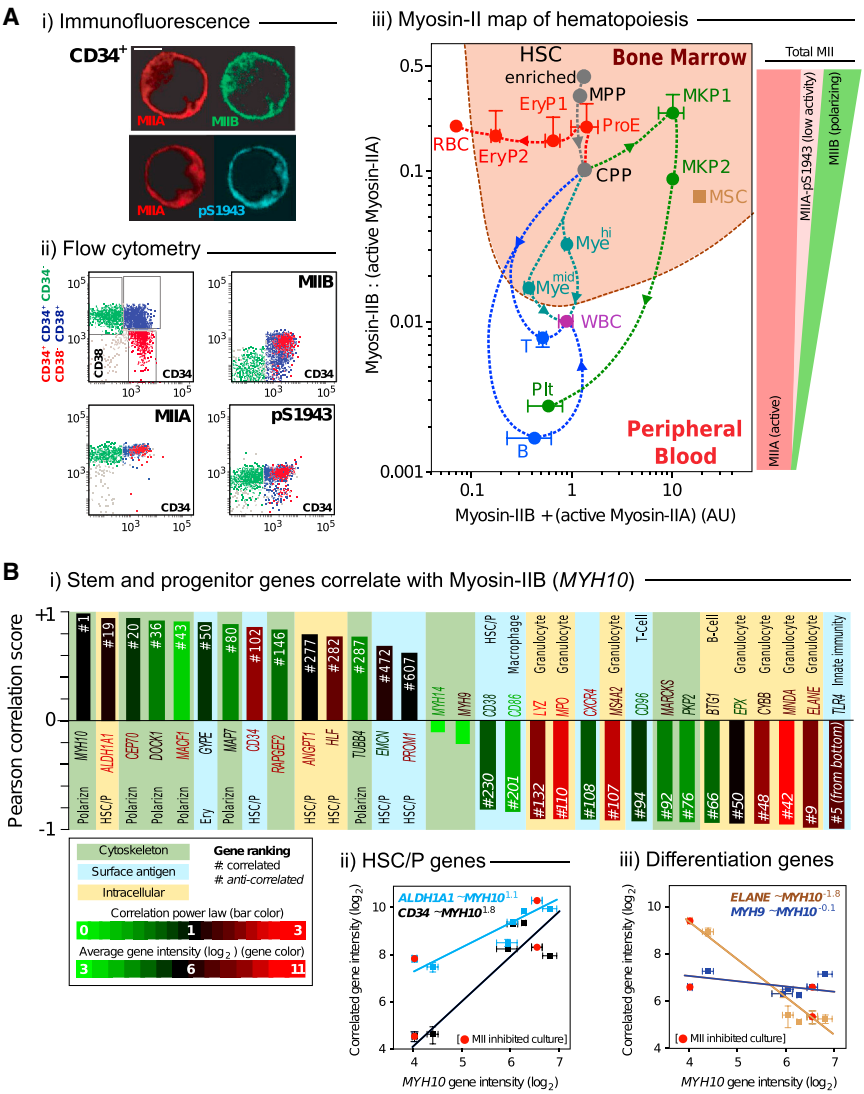

Figure 1. Two-Component Lineage Trajectories of MII Isoform States in Hematopoiesis

(A) MIIB relative to active fraction of MIIA (non-phosphorylated MIIA), transformed to a measurable B:A ratio versus sum total intensity (a.u.). (Ai) Images of coimmunostained MIIA and MIIB (bars = 5 μm). (Aii) Representative intracellular FACS dot plots show expression of MIIA, pS1943, and MIIB (y axis) across subpopulations (markers indicated in x axis). (Aiii) Mean fluorescent intensity of MIIs for each subpopulation from flow cytometry was normalized to an internal fluorescence control (A549), and B:A was calibrated to an absolute ratio from mass spectrometry analyses of MSCs (B:A = 6:94). The perforated endothelium schematically illustrates the permeable barrier between bone marrow and circulating cells. MKP, MK Progenitor 1 ($CD34^+CD41^+$), 2 ($CD34^-CD41^+$); ProE, Proerythroblast ($CD44^+GPA^-$); EryP, Erythroid Progenitor 1 ($CD44^+GPA^+$), 2 ($CD44^-GPA^+$); Plt, Platelet; T, B, Lymphoid; Mye^{mid}, Mye^{hi}, Bone marrow $CD33^+$ myeloid. WBC: Mean result for PB. Mean ± SEM of $n \geq 3$, with errors bars omitted if <5% of mean.

(B) Key genes correlated with *MYH10* and ranked by |Pearson correlation| > 0.75 or fit with a power-law. (Bi) Data sets were derived from RMA summarized microarray analyses of fresh populations of HSC-enriched, MPP, CPP, and cultured $CD34^+$-derived cells control or treated with Blebb (see Supplemental Experimental Procedures). Colors in bar graphs and gene symbols respectively represent power law exponents or gene intensities, and they are normalized by minimum levels (green: 0 or $\log_2 3$) and maximum levels (red: 3 or $\log_2 11$) of correlated genes using *MYH10* as a reference (black: 1 or $\log_2 6$). Representative correlation plots between *MYH10* and HSC/P (Bii) or differentiation (Biii) gene markers are shown (mean ± SEM of $n \geq 2$).

See also Figure S1, Table S1, and Table S2.

more slowly from F-actin than MIIA, resulting in higher force generation per MIIB (Wang et al., 2003). However, MIIB in human ESCs or stem cells in general has unknown functions. MIIC appears restricted to epithelial cells (Ma et al., 2010) and serves here as a useful negative control in expression analyses. Here, we reveal critical roles of MIIA and MIIB in adult hematopoiesis and use that understanding to enrich highly heterogeneous HSC/Ps for long-term hematopoietic stem cells.

RESULTS

MII Isoforms Switch from B-and-A to Only A in Human Adult Hematopoiesis

Immunofluorescence of human $CD34^+$ cells reveals cortical MIIB as well as MIIA (Figure 1Ai), but flow cytometry and immunoblots show that myosin levels vary with surface markers and also across differentiated lineages (Figure 1Aii, Figures S1A and S1B, available online). Mass spectrometry-calibrated intracellular flow (MS-IF) cytometry (Figure S1C, Supplemental Experimental Procedures) was developed to quantify absolute isoform stoichiometry, which is not possible by antibody methods alone due to differential sensitivities of antibodies to isoforms. MS-IF cytometry of diverse hematopoietic cell types reveals that MIIB is no more than ~30% of total MII across cell types and has a large dynamic range of ~5,000-fold compared to ~80-fold for MIIA (Table S1). However, MS also revealed MIIA phosphorylation at S1943 (pS1943), which deactivates MIIA through myofilament disassembly (Dulyaninova et al., 2007), and so a phosphospecific antibody was used to estimate the pS1943 stoichiometry of MIIA through a calibration scheme using mutant GFP-MIIA (see Supplemental Experimental Procedures). Based on this, ~50%–60% of MIIA is phosphorylated as pS1943 in the three key HSC/P subpopulations of $CD34^+$ cells (Figure S1D) per standard surface markers (Majeti et al., 2007; Novershtern et al., 2011):

{"HSC enriched" cells: $CD34^+$, $CD38^-$, $CD90^+$, $CD45\text{-}RA^-$, $CD133^+$}
{Multipotent progenitor ("MPP"): $CD34^+$, $CD38^-$, $CD90^-$, $CD45\text{-}RA^-$, $CD133^+$},

{"Common potent progenitor ("CPP"): $CD34^+$, $CD38^+$, $CD90^-$, CD45-RA^+, $CD133^-$}.

In differentiation, pS1943 generally decreases as MIIA is activated (Figure S1D), except for MKs in which pS1943 is similarly high as in HSC/Ps.

Phosphorylation at S1943 is equivalent to inhibiting ~50% of MIIA activity (Raab et al., 2012), so that for any cell type, *active*-MIIA = (50% of total MIIA) × (1 + MIIA fraction of *non*-pS1943). The result for *active*-MIIA proves to be nearly constant throughout hematopoietic differentiation and makes a useful common denominator. As such, a myosin map of hematopoiesis shows the highest stoichiometric ratio of (MIIB: *active*-MIIA) ≈ 1:2 (50%) in "HSC-enriched" (Figure 1Aiii) and a ratio of (MIIB: *active*-MIIA) ≥ 1:10 for the other marrow-restricted cells that include nucleated erythroid progenitors, MKs, and nonhematopoietic MSCs. For cell types that predominantly exit the marrow, the ratio (MIIB: *active*-MIIA) generally decreases as MIIB is specifically repressed—except for red blood cells (RBCs), which repress both myosins in similar proportion. Hematopoietic differentiation thus involves a major switch from MIIB + MIIA to active MIIA alone.

The programmatic nature of MII changes in hematopoiesis is evident in the fact that all nine of the marrow-resident cell types measured here cluster together in the MII map (Figure 1Aiii). Based on the "marrow" space in such a map being roughly half as large as that spanned by all measured cell types, we estimate a clustering probability $p \approx (1/2)^{11}(1/2)^5 = 0.000015$. This high significance p provides a metric of the systematic consistency of our MII measurements in addition to revealing a broad MII program.

Since MIIB was highest at the protein level in $CD34^+$ subpopulations, microarray profiling of the different stem/progenitor/differentiated cells allowed us to identify genes that correlate with expression of *MYH10* (Figure 1Bi). *CD34* correlated strongly with *MYH10* in showing a power law exponent of 1.8 (Figure 1Bii), whereas the differentiation gene *ELANE* is strongly anticorrelated with a power law of −1.8 exponent (Figure 1Biii). *MYH9* shows no correlation with *MYH10*. Transcripts that fit well were further assessed with a second, novel algorithm for a robust list (Table S2). A key subset is ranked on the correlation with *MYH10* and color-coded for the power law. Consistent with protein-level analyses, both *MYH9* and *MYH10* transcripts are of similar (midrange) intensity. About 1% of *MYH10*-correlated genes are known HSC/P markers, while >10% of the most anticorrelated genes are specific lineage markers. The profiling indeed shows maintenance of HSC/P markers (e.g., *CD34* and *ALDH1A1*) and suppression of differentiation genes (e.g., *ELANE*) (Figures 1Bii and 1Biii). Transcriptome dynamics thus align well with protein dynamics along with the differentiation trajectory.

MIIB Polarization in Marrow-Derived $CD34^+$ Cells

Some of the *MYH10*-correlated genes (*CEP70*, *DOCK1*, *MACF1*, *MAP7*, and *TUBB4*) not only polarize but also have roles in motility via the microtubule system. MIIB might be more cortical than MIIA in round, uncultured $CD34^+$ cells (Figure 2A), and in the ~50% of $CD34^+$ cells that are polarized in culture, MIIB is clearly enriched in the uropod by 75%, while MIIA is diffuse and uniform. The microtubule organizing center (MTOC) was also in the uropod as expected (Giebel et al., 2004). However, because cytoskeletal polarization in MSCs is suppressed by soft microenvironments (Raab et al., 2012), it became important to measure the elasticity of intact BM. Therefore we sectioned fresh bone lengthwise to expose the marrow for probing by atomic force microscopy. We determined a microscale elasticity of ~0.3 kilopascal (kPa) (Figure 2B), which is $>10^6$-fold softer than rigid bone and plastic. HSC/Ps have also been seen to localize at or near the osteoblastic endosteum of bone, which we had previously measured to have an elasticity >30 kPa (Engler et al., 2006). The softness of marrow is likely a product of both high cellularity and low extracellular matrix density: fibronectin (FN) is ubiquitous in marrow but is denser near the endosteum where collagen-I is also high (Nilsson et al., 1998). $CD34^+$ cells clearly anchor specifically to FN versus collagen-I (Figures S2A–S2C), and so we FN-functionalized gels of polyacrylamide to test matrix elasticity effects on MIIB polarization. Similar to our findings for marrow-derived MSCs (Raab et al., 2012), MIIB polarization in $CD34^+$ cells is suppressed in cultures on marrow-mimetic soft matrix but promoted in cultures on endosteum-mimetic stiff matrix (Figure 2C). Blebb rapidly abolishes MIIB polarization on stiff matrix without affecting membrane intensity of MIIB. MII activity and stiff matrix (including rigid plastic if cells adhere) thus drive polarization in $CD34^+$ cells.

Local stresses independent of adhesion can polarize MII in *Dictyostelium* cells that are pulled into micropipettes by aspiration (Ren et al., 2009). Hematopoietic cells were likewise aspirated at low stress (<1 kPa) after transfection of GFP-MIIA or MIIB, and within just 20 min, MIIB polarized by more than 10-fold into the stressed projection (Figure 2D), while MIIA polarized much less. Importantly, receptors such as integrins do not engage the micropipette wall, and so polarization can indeed be independent of adhesion. Partial knockdown of MIIB in $CD34^+$ cells followed by aspiration also showed greater distension of the membrane as well as membrane fragmentation (Figure 2E), and knockdown cells also showed an ~20% decrease in migration through a 3 μm pore filter (Figure S2D). Functionally, MIIB polarization in $CD34^+$ cells is thus protective of membrane shape changes produced by cell forces.

Asymmetric Division Is Biophysically Regulated by MIIB

Large cortical tensions are generated in cells as they round up and divide during asymmetric division (Sedzinski et al., 2011). Because *MYH10* correlates with a half-dozen genes involved in asymmetric division of hematopoietic cells (Ting et al., 2012) (Table S3), confocal imaging and partial knockdown (Figure 3Ai) were used to assess MIIB in asymmetric division of $CD34^+$ cells (Figure 3Aii), which occurs in ~30% of cells (consistent with Lordier et al., 2012). MIIB enriches toward the $CD34^{hi}$ daughter cell, concentrating near the cleavage furrow by ~3-fold (Figure 3B), whereas CD34 appears segregated between cells but otherwise locally homogenous, consistent with lateral mobility of this membrane protein. The results suggest that high cortical tensions in the cleavage furrow have a similar effect on receptor-independent localization of MIIB as that of local stressing by a micropipette.

Please cite this article in press as: Shin et al., Contractile Forces Sustain and Polarize Hematopoiesis from Stem and Progenitor Cells, Cell Stem Cell (2014), http://dx.doi.org/10.1016/j.stem.2013.10.009

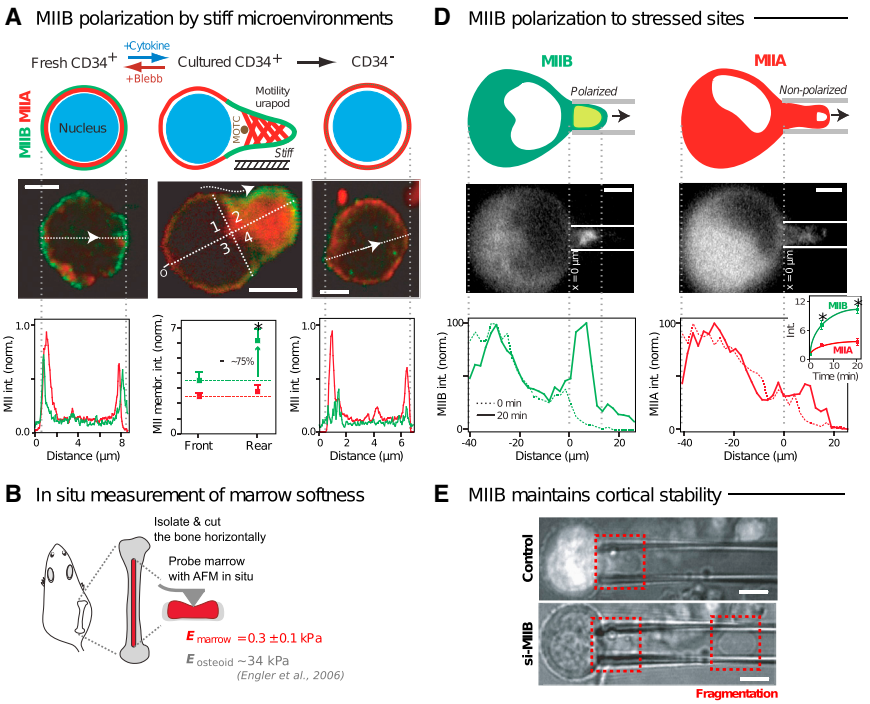

Figure 2. MIIB Is Polarized in Motile CD34$^+$ Cells and Localizes to Where Cells Are Stressed

(A) MIIB is more membrane-localized than MIIA in CD34$^+$ cells before and after serum-free culture, but not in CD34$^-$ cells. Bar = 5 μm. For the left and right panels, protein intensity was measured across the cell diameter (representative images and diameters are shown). For the middle panel, cortical intensity was measured clockwise (arrow) from the front of the cell origin ("0"). "Front" is the summed intensity over contour in the first and fourth quadrants (~50% of the total contour), while "Rear" is the summed intensity over the remaining contour.

(B) Measurement of in situ marrow elasticity by atomic force microscopy (AFM). Young's modulus E_{marrow} is obtained from indentation measurements performed at different locations across the exposed marrow samples. The force versus indentation curves are fit by $F = E\,\delta^2\,(2/\pi)\,(tan\,\alpha)/(1-\nu^2)$, where δ is the indentation, ν is the Poisson ration (assumed to be 0.5), and α is the half opening angle of the AFM tip (Sneddon, 1965). From 88 measurements done on four mouse tibia or femur samples, E_{marrow} = 0.32 ± 0.07 kPa.

(C) Arrows indicate direction of intensity measurement as described for Figure 2A middle panel.

(D) Stress-induced localization of mCherry-MIIB and less so GFP-MIIA are demonstrated in micropipette aspiration of MEG01 cells. Yellow region in cartoon represents MII accumulation and white regions represent MII^{lo} areas. Representative images and intensity measurements across cell midline are shown with the inset kinetics of MIIA and MIIB intensities normalized by the intensity at t = 0 min. (Pressure Δp = 1 kPa; bar = 10 μm).

(E) MIIB maintains cortical stability of CD34$^+$ cells, based on aspiration of cells with or without knockdown with si-MIIB. (Δp = 1 kPa; bar = 5 μm). For all image analyses, n ≥ 10 each sample, two donors, mean ± SEM, and *p < 0.05. See also Figure S2.

Partial knockdown of MIIB abolishes the asymmetry and also the segregation of CD34 (Figure 3B, bottom). Whereas asymmetric division of CD34$^+$ cells results in 6-fold higher MIIB in the CD34$^+$ daughter than in the CD34$^-$ daughter, knockdown decreases the MIIB level in CD34$^+$ to that in CD34$^-$ and suppresses asymmetric division (Figure 3C). Prolonged cultures of MIIB knockdown cells increase the relative number of CD34$^+$ progenitors with more colony forming unit-granulocyte and macrophage (CFU-GM) (Figure 3D), consistent with MIIB regulating asymmetric division when late CD34$^+$ progenitor cells transition to CD34$^-$ cells and when CD34 molecularly segregates between daughter cells. Tracking of division using carboxyfluorescein diacetate succinimidyl ester (CFSE) (Hawkins et al., 2007) shows that partial knockdown of MIIB increases the number of CD34$^+$CD38$^-$ cells by 2-fold (Figure 3Ei) or for CD34$^+$CD38$^+$ cells by 1.5-fold (Figure 3Eii), whereas CD34$^-$ numbers remain unaltered (Figure 3Eiii). On the other hand, partial MIIA knockdown (~30%) did not alter numbers of any subpopulations (Figure S2E). The data reveal MIIB as a major factor in asymmetric division and differentiation of CD34$^+$ cells to CD34$^-$ cells.

MIIA Dephosphorylates in Differentiation to a Mechanically Active State

MIIA is often the dominant MII isoform and can influence MIIB (Raab et al., 2012), which implies that phosphoregulation of MIIA can in principle influence hematopoiesis (Figure 4A). We therefore examined regulation by niche factors of pS1943 in CD34$^+$ cells and found the highest levels of pS1943 in uncultured CD34$^+$ cells (Figure 4Bi; Figure S1D), with levels systematically decreased upon differentiation with Thrombopoietin (Tpo) and Granulocyte-Colony Stimulating Factor (G-CSF), but not Stem Cell Factor (SCF) alone (Figure 4Bii). Transforming Growth Factor-β (TGF-β) promotes HSC hibernation (Yamazaki et al., 2011) and blocks the decrease in pS1943 with cytokines (Figure 4B). Remarkably, Blebb mimics TGF-β (Figure 4B). In contrast, very low pS1943 in myeloid CD33$^+$ cells (Figure S1D) and in the human monocytic cell line (THP-1) are consistent with rapid proliferation of THP-1 in suspension (which can be blocked by Blebb). Both CD34$^+$ and CD34$^-$ cell numbers anti-correlate with the level of pS1943, and the half-maximal effect was observed at ~35% pS1943-MIIA (Figure 4B). MIIA is thus modulated by cytokines critical to precirculation differentiation.

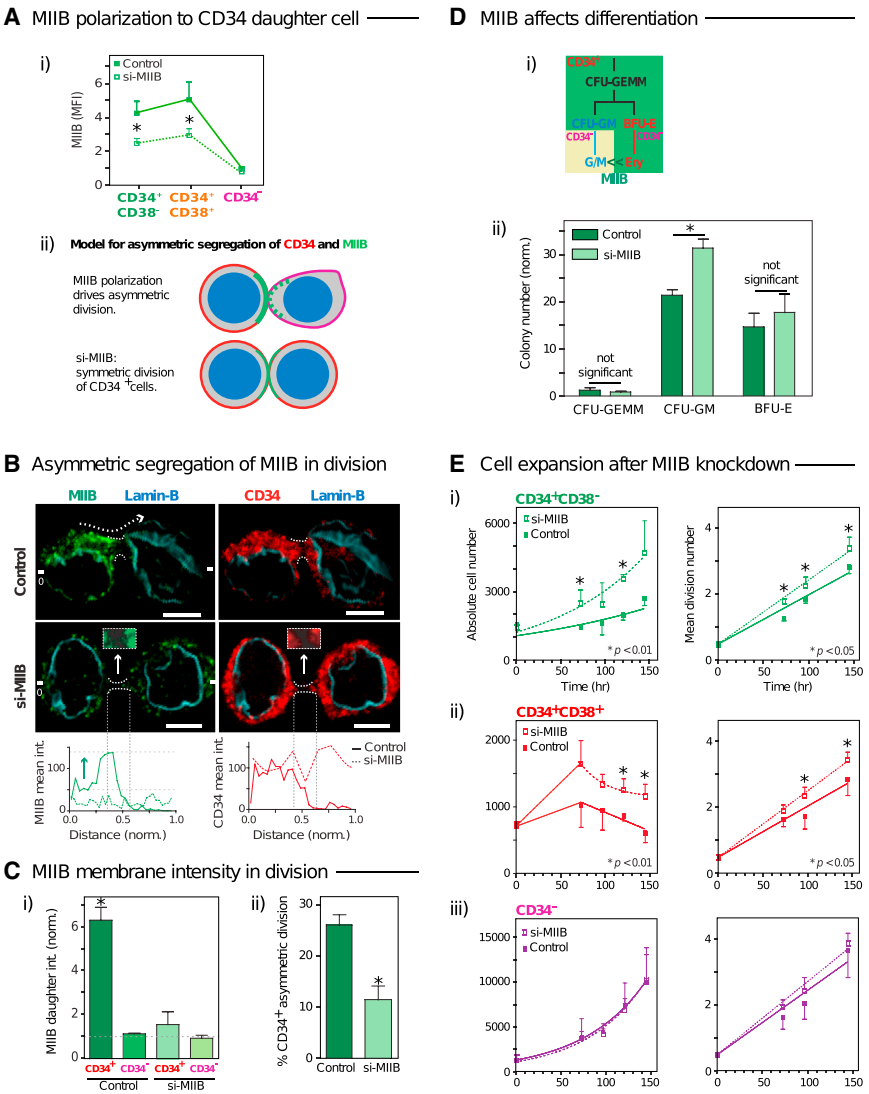

Figure 3. MIIB Polarizes in and Promotes Asymmetric Division of CD34$^+$ to Differentiated Cells

(A) Partial knockdown of MIIB decreases protein by ~40% in CD34$^+$CD38$^-$ and CD34$^+$CD38$^+$. (Ai) Mean Fluorescence Intensity (MFI) of MIIB protein was measured by flow cytometry. (Aii) Hypothetical model for asymmetric segregation of CD34 and MIIB in division shown for WT versus MIIB knockdown.

(B) MIIB segregates asymmetrically in dividing CD34$^+$-derived cells unless MIIB is knocked down (top). Bar = 5 μm. Intensities of MIIB and CD34 were measured (bottom) along the membrane contour of dividing cells from "0" through the cleavage furrow to the antipole, with distance normalized by total length. A green arrow indicates the difference in MIIB intensity between periphery and cleavage furrow.

(C) MIIB membrane intensity bifurcates to CD34^{hi} and CD34^{lo} daughters in dividing cell pairs (Ci), unless MIIB is knocked down. Percentage of asymmetrically dividing CD34$^+$ cells is suppressed with MIIB siRNA versus control (Cii). Greater than forty cells per group.

(D) Colony forming assays after 3 days in methylcellulose medium supplemented with cytokines. (Di) A relationship among different progenitors in terms of CD34 and MIIB expression. (Dii) CFU-GM increases with MIIB knockdown.

(E) Absolute CD34$^+$ cell numbers expand after MIIB knockdown, with normalization to an initial total of 10,000 cells (left), and CFSE tracking shows an increase in mean division number per time (right). Slopes for si-MIIB are as follows: control, (0.02: 0.015) for CD34$^+$CD38$^-$ (Ei) and CD34$^+$CD38$^+$ (Eii), and (0.02: 0.02) for CD34$^-$ (Eiii). For all graphs, *p < 0.05 between Control (= Scrambled) versus MIIB siRNA for each data point, mean ± SEM, and n ≥ 3 donors.

See also Figure S2 and Table S3.

Fresh CD34$^+$CD38$^-$ are softer than CD34$^+$CD38$^+$ (Figure 4Ci), and consistent with the high pS1943-MIIA in CD34$^+$ cells, cells transfected with a site-specific MIIA phosphomimetic mutant (S1943D) fragment more often (from a weak cortex) and also divide more slowly compared to wild-type controls (Figures 4Cii and 4Ciii). These functional results all indicate that high pS1943-MIIA impacts cell mechanics and limits cell division, and hence, differentiation. Transcriptional profiles reveal perturbation of pathways that regulate MIIA phosphorylation in CD34$^+$ cells by Blebb (Table S4). Matrix mechanics therefore have an understandable effect on pS1943-MIIA as well (Figure 4Di): soft FN-coated gels (20 μg/ml) maximize pS1943 in CD34$^+$ cells treated with cytokines compared to stiff matrix, while CD34$^-$ cells appear unaffected (Figure 4Dii). This response to stiff matrix is blocked with the phosphomimetic, deactivating S1943D-MIIA (Figure 4Diii). Increased cell spreading as part of matrix engagement on stiff substrate thus requires MIIB in CD34$^+$ cells (Figure 2C), whereas differentiated cells use nonphosphorylated MIIA. At the same FN density as above, the number of CD34$^+$ CD38$^-$ is 4-fold higher on soft matrix relative to stiff matrix (but Blebb eliminates the difference), whereas the number of CD34$^+$CD38$^+$ remains constant (Figure 4E). CD34$^+$CD38$^-$ cells are thus sensitive to matrix elasticity, with sensitivity modulated by MII.

In Vivo Roles in HSC/Ps: MIIB Contributes to Differentiation, whereas MIIA Confers Survival

Based on our in vitro results, a major knockdown of MIIB in human cells grafted into BM should repress asymmetric division and lead to (1) an accumulation of human cells in marrow and (2) a suppression of circulating human blood cells. To test this hypothesis, fresh human CD34$^+$ BM cells were transduced with shRNA-carrying lentivirus to knock down MIIB, which was followed by puromycin selection of transduced cells. Cells were injected directly into bone of NOD/SCID/IL-2Rγ$^{-/-}$ (NSG) mice to study BM retention both at 16 hr and at 20 weeks (Figure 5Ai); this same duration has been described by others (Notta et al., 2011) as providing "a stringent test of long-term

Please cite this article in press as: Shin et al., Contractile Forces Sustain and Polarize Hematopoiesis from Stem and Progenitor Cells, Cell Stem Cell (2014), http://dx.doi.org/10.1016/j.stem.2013.10.009

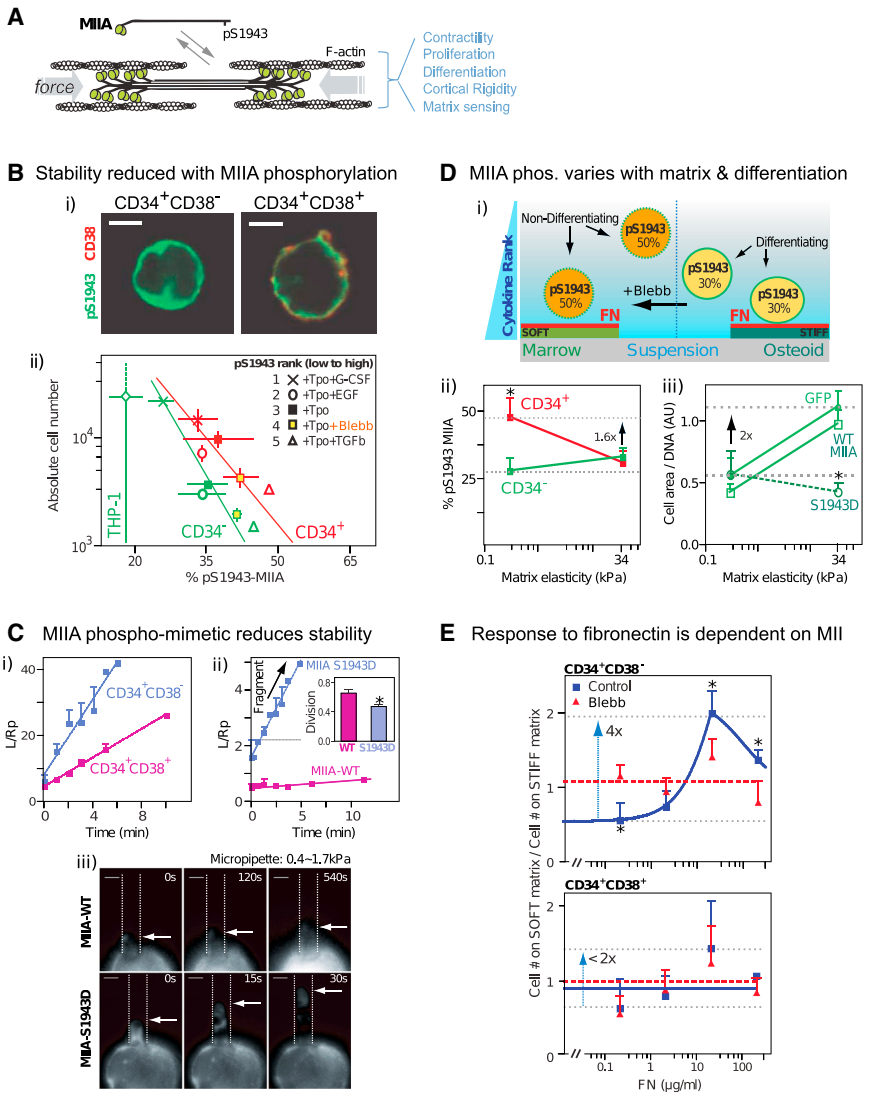

Figure 4. Phosphorylation of MIIA Regulates the Biophysics of CD34$^+$ Differentiation

(A) Dephosphorylation of MIIA at S1943 promotes assembly and function.

(B) CD34$^+$ differentiation with soluble factors decreases pS1943. (Bi) Representative images showing pS1943 expression in fresh CD34$^+$ cells. Bar = 5 μm. (Bii) pS1943 (normalized to MIIA) was measured by flow cytometry [n = 3 donors, ± SEM; fit to Log Y = aX + b (a,b): (CD34$^+$: −0.05, 5.74; in red), (CD34$^-$: −0.10, 6.74; in green)]. Minimum pS1943 per MIIA was measured for THP-1 cells (0.07 ± 0.01). All cells were treated with SCF and indicated cytokines. pS1943% values were normalized as described in Figure S1D (n = 3, ± SEM). pS1943 percentage for SCF only = ~40%.

(C) MIIA S1943D phosphomimetic decreases both cortical stiffness and cytoskeletal stability. Aspiration length L, normalized by pipette radius, Rp (L/Rp), versus time for various cells with (*slope, intercept, effective viscosity* η) were as follows: (Ci) CD34$^+$CD38$^-$ (5.7/min, 8.3, 3.2 Pa/s) and CD34$^+$CD38$^+$ (2.2/min, 4.7, 8.5 Pa/s); (Cii) MIIA-WT: (0.02/min, 0.5, 1,400 Pa/s), MIIA-S1943D (0.70/min, 1.6, 40 Pa/s). n = 5, ±SEM. The inset bar graph in (Cii) shows the fraction of transfected COS-1 cells after MIIB knockdown that undergo cell division (2n and 4n cells) as calculated by subtracting the fraction of polyploid cells (n = 3, ±SEM, *p < 0.05). (Ciii) Representative images of aspiration of transfected COS-1 cells (bar = 10 μm).

(D) CD34$^+$CD38$^-$ cells sense matrix elasticity with changes in pS1943-MIIA similar to cytokines (Di). (Dii) Soft matrix maintains high pS1943 in CD34$^+$. *p < 0.05 (three donors, ±SEM). (Diii) pS1943 limits matrix sensing: cell area was normalized to DNA to correct for ploidy of COS-1. *p < 0.05 for GFP-S1943D 34 kPa versus GFP or GFP-MIIA 34 kPa (n ≥ 20, ±SEM).

(E) CD34$^+$ numbers on soft matrix (0.3 kPa) scaled by stiff matrix (34 kPa) increase with fibronectin (FN) density unless MII is inhibited. For CD34$^+$CD38$^-$, EC_{50} ~22.4 μg/ml, *p < 0.05 (n ≥ 3, ±SEM).

See also Table S4.

repopulation'' of human xenografts injected into the femurs of NSG mice for which ''HSCs were operationally defined by lymphomyeloid engraftment that persisted for at least 20 weeks after transplant.'' Standards for mouse HSCs differ from those of human (Doulatov et al., 2012), but 12–16 weeks is currently considered as ''long-term engraftment'' (Oguro et al., 2013). We injected directly into marrow rather than into blood to avoid any potential effect of knockdown on trafficking from blood to marrow. Human cells in mice were identified by dual immunostaining for hCD45 and hCD47 (Figure S3A), since human RBC and platelets do not express hCD45 while hCD47 confers immunocompatability to all human cells within NSG mice (Rodriguez et al., 2013; Takenaka et al., 2007). Partial permanent MIIB knockdown (by ~40%) (Figure 5Aii) leads to 3-fold greater retention of cells in marrow when they are assayed just 16 hr after marrow injection (Figure 5Bi); this could reflect the fact that knockdown impairs migration through constraining micropores by 20% ($p < 0.05$; Figure S2D). Despite this initial retention advantage, the percentage of human peripheral blood (PB) cells in circulation at 6 weeks after transplantation is 7-fold lower for the MIIB knockdown cells (Figure 5Bii), and the difference is maintained after 20 weeks (Figures 5Ci and 5Cii). Sustained engraftment is evident in control mice with significant human cell numbers in marrow and four of five mice showing human cells in PB. In contrast, MIIB knockdown cells were 6-fold more abundant in marrow, but only one of five mice had human cells in circulation. MIIB is thus required to generate PB cells.

Because MIIA is the dominant isoform in hematopoietic cells and is phosphoregulated distinctly in marrow cells versus PB cells, we characterized MIIA contributions to hematopoiesis by performing competitive transplants of BM from tamoxifen-inducible cre-*Myh9* knockout mice. These conditional knockout cells (with surface marker CD45.2) were mixed 1:1 with cells from

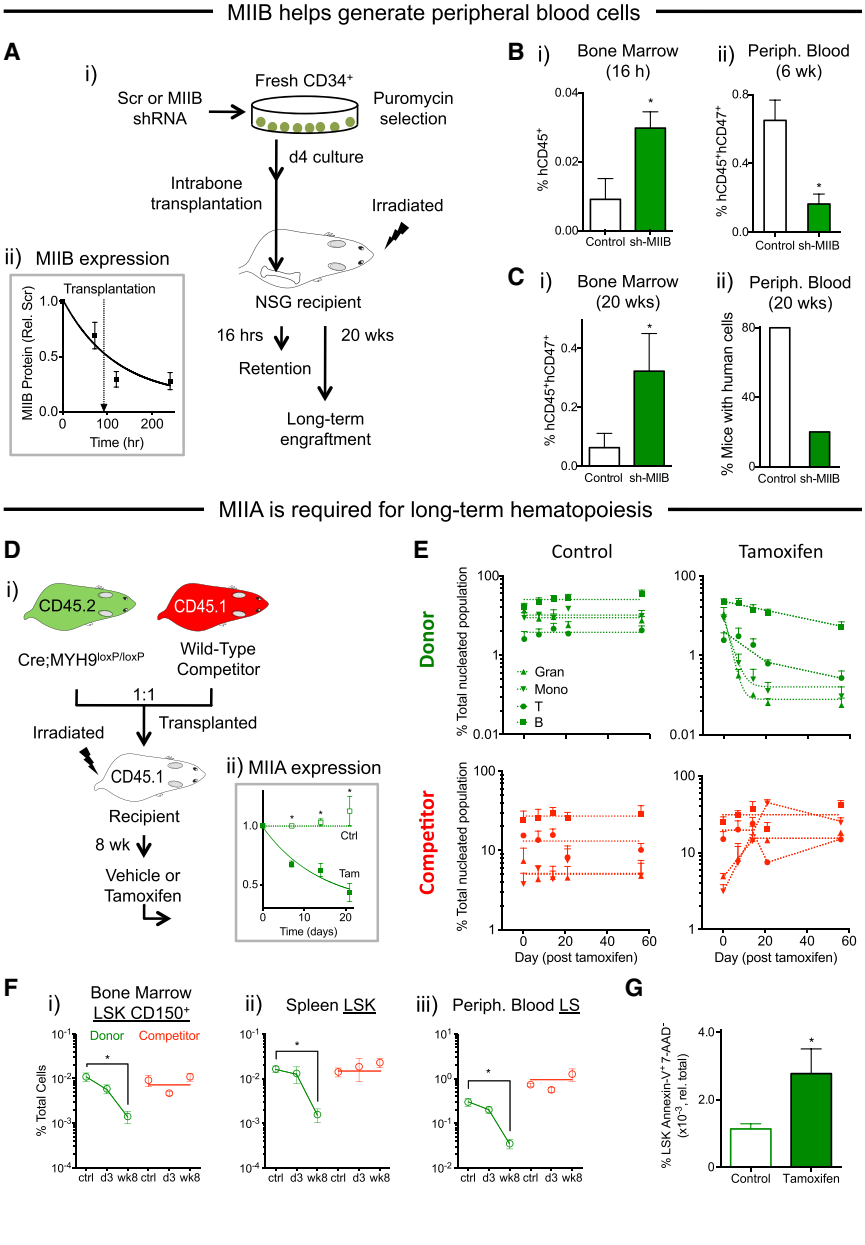

Figure 5. MII Isoforms Regulate Hematopoiesis In Vivo

(A) Scheme for in vivo experiments to test MIIB functions (Ai). (Aii) MIIB expression kinetics with shRNA knockdown relative to control. $t_{1/2}$ = 81 hr. n = 5 mice for each group (±SEM for all graphs), transplanted via an intratibial route with 5 × 10^3 BM $CD34^+$ cells per sublethally irradiated mouse. Transplantation occurred 4 days after lentiviral transduction, with 2 days puromycin selection.

(B) MIIB knockdown increases short-term (16 hr) retention in bone marrow (BM) (Bi), but decreases short-term (6 week) generation of peripheral blood (PB) (Bii). *p < 0.01 control (scrambled) versus MIIB shRNA.

(C) MIIB knockdown increases long-term (20 weeks) BM engraftment (Ci), but suppresses PB generation (Cii). For PB generation, the number of positively engrafted mice is shown (≥0.1% total nucleated cells).

(D) Scheme for in vivo experiment to test MIIA functions (Di). BM cells from Cre:$Myh9^{loxP/loxP}$ (CD45.2) and from WT competitor (CD45.1) were transplanted at a 1:1 ratio into lethally irradiated WT recipients. (Dii) Eight weeks after reconstitution, mice were treated with tamoxifen to delete *Myh9* as assayed by protein expression (*p < 0.01, control versus tamoxifen, n ≥ 3, ±SEM for all graphs). Deletion occurred with $t_{1/2}$ = 9.6 days. n ≥ 8 mice for each group from two independent experiments (±SEM for all graphs).

(E) PB lineages with deleted *Myh9* are lost from circulation with kinetics similar to clearance of WT cells. The donor (top) and competitor (bottom)-derived granulocyte (Gran, $Gr\text{-}1^+Mac\text{-}1^+$, larger side scatter), monocyte (Mono, $Gr\text{-}1^+Mac\text{-}1^+$, smaller side scatter), T cell (T, $CD3^+$), and B cell (B, $B220^+$) lineages in PB were quantified at the indicated time points after vehicle (left) or tamoxifen (right) treatment. Decay half-lives for tamoxifen-treated donor Gran, Mono, T, and B are 1.3, 1.7, 24.2, and 18.8 days, respectively

(F) *Myh9* deletion decreases HSC/P subpopulations across different hematopoietic organs in the long term (8 weeks), but not in the short term (3 days). Donor and competitor HSC/P cells were quantified in BM ($LSKCD150^+$, Fi), spleen (LSK, Fii), and PB (LS, Fiii) (control versus treated, *p < 0.01).

(G) *Myh9* deletion increases apoptosis of LSK. Treatment was for 3 days (*p < 0.01).

wild-type mice (CD45.1) and injected into sublethally irradiated recipient mice (CD45.1) (Figure 5Di). This knockout strategy with mouse cells instead of human cells proved necessary for understanding MIIA because our in vitro results for proliferation indicated no effect with partial knockdown of MIIA in contrast to major defects with MIIB partial knockdown (Figure 3A). At 8 weeks after transplantation of the mixed cells, the total percentage of donor and competitor blood cells was ~50% each, and upon tamoxifen treatment, MIIA decreased as expected only in CD45.2 donor cells (Figure 5Dii). In PB, donor myeloid cells decreased rapidly compared to lymphoid cells ($t_{1/2}$ = ~30–40 hr versus ~20–25 days) (Figure 5E), but these half-lives are within 2-fold of those reported for both myeloid (Basu et al., 2002; van Furth and Cohn, 1968) and lymphoid (Fulcher and Basten, 1997; Sprent and Basten, 1973) lineages in mouse blood. MIIA loss therefore does not greatly affect viability of terminally differentiated lymphoid cells, while blood cell production from progenitors is clearly suppressed. Consistent with this, we find in BM that Lin^- $Sca\text{-}1^+$ $c\text{-}Kit^+$ (LSK) $CD150^+$ cells (which include progenitors or HSC/Ps; Kiel et al., 2005) are reduced 10-fold at just 8 weeks after *Myh9* deletion (16 weeks since transplant), with similar results for LSK in spleen and LS in blood (Figures 5Fi, 5Fii, and 5Fiii, respectively). MIIA is thus required for sustained engraftment in vivo and hematopoiesis. An early apoptotic fraction (Annexin-V^+ and 7-AAD^-) of the LSK population also increased just 3 days after *Myh9* deletion (Figure 5G), although the total LSK number remained unchanged at this time point (Figure 5F). Irreversible loss of MIIA therefore suppresses differentiated cell numbers in the long term as defective HSC/Ps progressively apoptose.

Please cite this article in press as: Shin et al., Contractile Forces Sustain and Polarize Hematopoiesis from Stem and Progenitor Cells, Cell Stem Cell (2014), http://dx.doi.org/10.1016/j.stem.2013.10.009

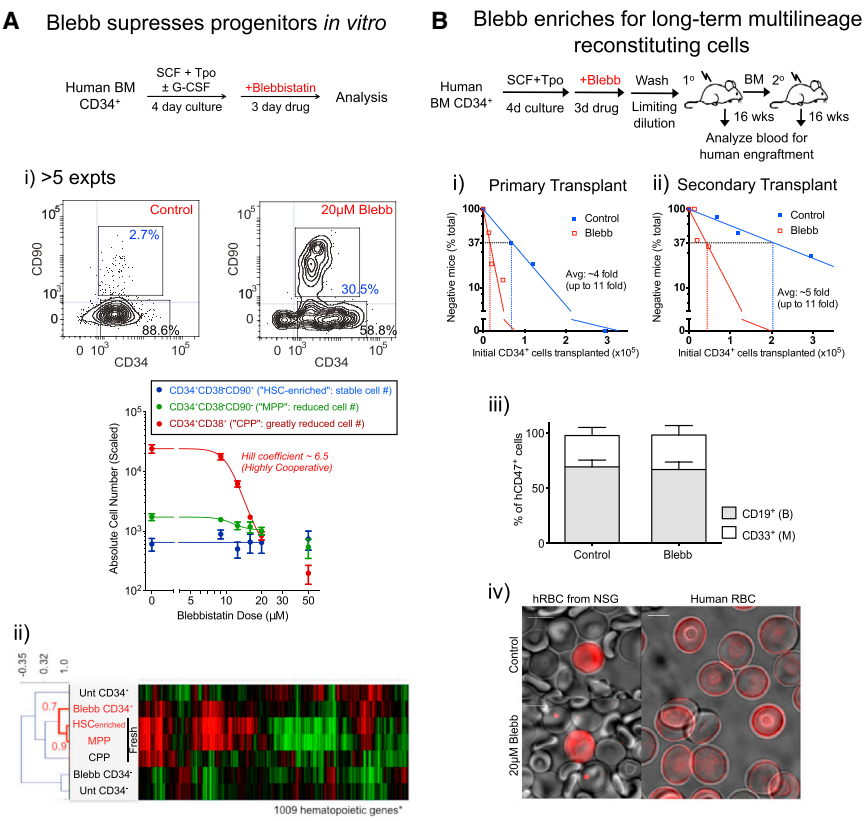

Figure 6. MII Inhibition Maintains HSC-Enriched Population with Long-Term Multilineage Reconstitution Potential

(A) Scheme for in vitro experiments (top). (Ai) Representative flow cytometry contour plots for $CD34^+$ subpopulations, with dose-dependence of 2n cells showing 15.6- ± 4.1-fold enrichment at 20 μM Blebb. Absolute cell numbers were scaled to 10^4 initial cells and fit to dose-response curves: CPP and MPP IC_{50} = 10.5 μM; HSC-enriched numbers = 646 ± 77 (n ≥ 5 donors, ±SEM). These IC_{50} values are within ~2-fold of the inhibition constant K_i for pure MII (Kovács et al., 2004). (Aii) Blebb-treated $CD34^+$ cells show a gene expression profile similar to fresh $CD34^+CD38^-$ for hematopoietic genes (Table S4 and Table S5). Values are derived from two experiments.

(B) Limiting dilution serial transplant analyses show functional HSCs after myosin inhibition after 16 weeks (long-term). (Top) Scheme for in vivo experiments. (Bi) Limiting dilution primary transplant. The number of transplanted $CD34^+$ cells versus the percentage of unsuccessful engraftment determines the frequency of repopulating cells (n = 26 recipients per group from three independent experiments; $p < 0.0005$). (Bii) Secondary transplantation of BM from primary transplant demonstrates the maintenance of higher HSC frequency with Blebb compared to control (n ≥ 13 recipients per group, $p < 0.01$) (See Figure S3B). Transplantation with Blebb-exposed $CD34^+$-derived cells shows similar multilineage engraftment in the NSG mice compared to control cells, including myeloid ($CD33^+$), lymphoid ($CD19^+$) (Biii) (±SEM), and erythroid (GPA^+) (Biv). Bar = 5 μm.

(C) Kinetics of human-$CD41^+$ platelets in circulation were measured after transplantation of human $CD34^+$-derived cells and normalized by the initial number of $CD41^+$ cells transplanted. Areas under curves show significant differences between drug-treated and control. $p < 0.05$ in both phase I and phase II from at least nine recipients in three experiments (±SEM).

(D) Effects of Blebb on progenitors. (Di) Enrichment of polyploid MKs by Blebb (n = 4). y axis represents the ratios between polyploid MKs and 2n + 4n MKs. EC_{50} = 7.5 μM; Hill coefficient = 7.0. (Dii) Enrichment of BFU-E relative to CFU-GM in the absence of Epo, evaluated by colony forming assays. The maximum ratio was observed at 12.5 μM. IC_{50} = 10 μM, Hillslope = 5.0 (n = 3, ±SEM). (Diii) Sensitivity of erythroid progenitors to Blebb in the presence of Epo. BFU-E = $CD34^+IL\text{-}3R^+CD36^-$; CFU-E = $CD34^-IL\text{-}3R^-CD36^+$. Absolute values were normalized to 10^4 initial cell input and fit to dose-response curves. IC_{50}, Hill coefficient for CFU-E, 2n: 8.7 μM, −4.4 and 4n: 12.9 μM, −6.3; BFU-E, 2n: 10.9 μM, −9.7, 4n: 13 μM, 28, and Poly ≥ 8n: 0.2 μM, 2.0. (n = 2, ±SEM).

See also Figure S3, Table S4, and Table S5.

Transient Inhibition of MII with Blebbistatin Spares Only Long-Term Multilineage Reconstituting Cells

Blebbistatin is a reversible inhibitor of all MII isoforms, and dose-response studies of $CD34^+$ cultures show that it has a surprising but understandable effect: the diploid "HSC-enriched" population (as phenotypically defined per Majeti et al., 2007 and Novershtern et al., 2011) proves relatively stable to a 3-day treatment, which is long relative to the cell cycle, while the Blebb-treated MPP and CPP are depleted by 1.8-fold (±0.5) and 31-fold (±16), respectively. By suppressing only the progenitors and sparing the HSC-enriched population, the net effect is an enrichment of the latter among total $CD34^+$ cells by up to 16-fold (Figure 6Ai). Whole-genome transcript profiles indeed show that Blebb cultures correlate well with fresh HSC-enriched cells and MPP, but not CPP (Figure 6Aii, Table S4, and Table S5), whereas control $CD34^+$ cultures correlate with fresh CPPs. Blebb treatment beyond 3 days showed a progressive decrease in the HSC-enriched population, consistent with the conditional knockout studies above that suggest that MIIA is essential for hematopoiesis in vivo (Figures 5D–5F).

Functional tests of HSC enrichment by Blebb were conducted after washing out the drug and involved measuring the frequency of human cells in NSG mice after limiting dilution serial transplantations into multiple primary and secondary recipients (Figure 6B). A total duration of 32 weeks in primary plus secondary xenografts was chosen as sufficient to assess long-term

multilineage engraftment of human HSCs in NSG mice (Notta et al., 2011). Our blood analyses 16 weeks after primary transplantation showed that positive engraftment required fewer $CD34^+$ cells (~1 in 10,000) from Blebb-treated cultures compared to control cultures (Figure 6Bi; Figure S3B). If long-term multilineage engraftment were due solely to progenitors (such as MPPs), then the fact that Blebb-treated cultures have relatively fewer progenitors (Figure 6A) would have required that more (not fewer) Blebb-treated $CD34^+$ cells be injected for reconstitution. Both treated and control cultures also showed a similar percentage of human $CD34^+CD38^-$ and $CD34^+CD38^+$ populations in BM after transplantation (Figure S3D), indicative of engraftment, and Blebb results also compare well to uncultured $CD34^+$ cells in previous studies (Nishino et al., 2011). Sustained secondary engraftment provides an assay for cells with appropriate stem cell properties (Doulatov et al., 2012; Notta et al., 2011; Oguro et al., 2013) and our secondary transplantation results show that Blebb maintains a higher fraction of the HSC-enriched population compared to untreated cultures (~5-fold once again). Both treated and control human $CD34^+$ transplants produced a similar percentage of multilineage myeloid and lymphoid cells (Figure 6Biii) and a minor fraction of enucleated human RBCs in the NSG mice (Figure 6Biv). The latter were enriched by flowing blood through a microfluidic channel coated with anti-hCD47 and then staining for the erythroid-specific marker hGPA (Figure S3C).

MKs are unique among blood cells in being naturally polyploid and become more so in vitro with Blebb treatment, which also increases in vitro proplatelet formation (Shin et al., 2011). In the NSG mice, human platelets ($CD41^+$) showed two phases of circulation up to 2 weeks after transplantation that also seemed to benefit from Blebb treatments (Figure 6C). In phase I, human platelets are released into the circulation almost immediately and reach an initial peak between ~1–20 hr, consistent with intravenously infused MKs (Figure S3E) (Fuentes et al., 2010). Phase II peaks at ~20–90 hr and reflects a successful lodging of MKs in the marrow. Importantly, human cells treated with Blebb generate more human platelets per transplanted $CD41^+$ cell by about 4-fold in both phases, and shear forces appear to be important in regulating the size of human platelets derived from MKs (Figure S3F). Blebb indeed enriches for mature polyploid MKs in culture by ~10 fold (Figure 6Di). For other lineages, the sensitivity of individual progenitor lineages to Blebb proves cytokine dependent (Figure 5A; Figure S3G). For SCF and Tpo $CD34^+$-derived cells, the IC_{50} for CFU-GM is lower than that of BFU-E, with Blebb producing up to a 2-fold higher ratio of BFU-E to CFU-GM (Figure 6Dii). Erythroid lineages are thus preserved under non-Epo and submaximal MII inhibition. In contrast, when cells are cultured with Epo, both CFU-E and BFU-E numbers are reduced (Figure 6Diii). Functional studies thus reveal that short-term reversible MII inhibition in combination with specific cytokines enriches for HSCs, mature MKs, and even erythroid progenitors.

Sustained Blebbistatin Induces Apoptosis of Dividing $CD34^+$ Cells via Aryl Hydrocarbon Receptors and p53 Pathways

Control cultures show that CPP and MPP progenitors undergo 2- to 3-fold more divisions as expected compared to the phenotypically marked HSC-enriched population based on CFSE tracking (Figure 7A), whereas Blebb-treated cells (20 μM) do not divide. Decay rates of CFSE for $CD34^+$ subpopulations in either the presence or the absence of G-CSF (Figures S4A and S4B) indicate that Blebb accelerates decay, consistent with enhancing cell death. With the phenotypical HSC-enriched population, this is likely due to inhibition of cytokinesis of 4n cells trying to divide at the point drug was added. Apoptosis was measured by cleaved caspase-3 and increased 2-fold with Blebb (Figure 7B; Figures S4C–S4F), although G-CSF modulates survival (Figure 7B; Figure S4B). Suppression of MPP and CPP cell numbers with Blebb is therefore explained by cytokinesis-associated death, which seems consistent with similar roles for MII in apoptosis in *C. elegans* (Ou et al., 2010).

Transcription profiles of viable fractions from drug-treated and control cells implicate intersecting pathways that involve the aryl hydrocarbon receptor (AHR) and p53 (Table S4). AHR antagonists counteract apoptosis (Vaziri and Faller, 1997) and expand human HSC/Ps in culture (Boitano et al., 2010) (Figure S5A). The antagonist CH-223191 improves viability of both control $CD34^+$ and $CD34^-$ cells, specifically the cycling cells (4n) (Figure 7B). The number of apoptotic cells with Blebb treatment is also systematically decreased by the more potent StemRegenin-1 (SR1) (Figure 7C). Both CH-223191 and SR1 rescue $CD34^+$ cells from cell death by Blebb, since cell numbers approximate control conditions (Figure 7D; Figure S5B).

Total p53 protein was then assayed in the presence of Blebb and/or SR1. Total p53 protein increased ~2 fold with Blebb but reversed by SR1 (Figure 7E). Cyclic-pifithrin-α tests whether induction of apoptosis is dependent on p53-mediated transcription activity (Zuco and Zunino, 2008). The phenotypic "HSC-enriched" population is increased ~2-fold with cyclic-pifithrin-α in both control and Blebb-treated cells (Figure 7F) with an EC_{50} close to previous reports (30 nM) (Pietrancosta et al., 2005). AHR and p53 are thus implicated in Blebb-induced apoptosis.

DISCUSSION

Asymmetric division provides a means to maintain stemness while generating the many differentiated cells required for a tissue with high turnover such as blood (10^5 nucleated cells/s). However, it has been unclear as to how two interconnected daughter cells physically sort components to become distinct. While asymmetry of stem cell division in *C. elegans* is driven by its one isoform of MII (Ou et al., 2010), the mammalian homolog, MIIA, is expressed in many cells other than stem cells and unlike MIIB, MIIA polarizes very weakly if at all (Vicente-Manzanares et al., 2008; Raab et al., 2012). Compared to any other hematopoietic lineage, $CD34^+$ cells express the most MIIB relative to MIIA. MIIB polarizes strongly to regions of high cell tension or curvature where it can physically break the symmetry of cytokinesis (Sedzinski et al., 2011). It is therefore almost predictable that MIIB in $CD34^+$ cells will polarize near a cleavage furrow and define the $MIIB^{hi}$ daughter cell in asymmetric division (Figure 3). Since MIIB is localized near the membrane and is known to link to membrane proteins (Clark et al., 2006), $MIIB^{hi}$ could also help sort cell surface proteins such as CD34 and thereby correlate with $CD34^{hi}$ as seen. Depletion of MIIB from the $CD34^{lo}$ daughter cell is also propagated as a

Please cite this article in press as: Shin et al., Contractile Forces Sustain and Polarize Hematopoiesis from Stem and Progenitor Cells, Cell Stem Cell (2014), http://dx.doi.org/10.1016/j.stem.2013.10.009

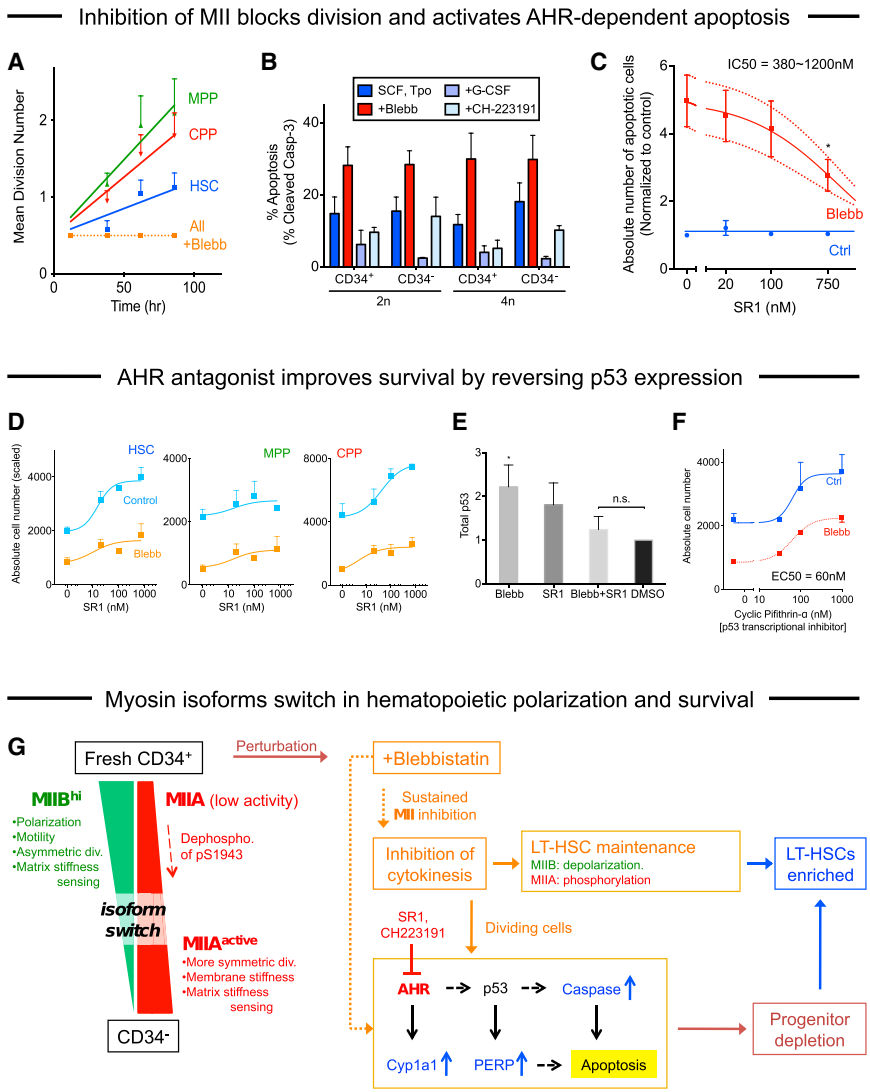

Figure 7. Inhibition of MII Blocks Division and Activates AHR-Dependent Apoptosis

(A) The mean division numbers for each HSPC subpopulation were calculated by fitting Gaussians to CFSE data, and Blebb blocks division ($n \geq 3$ donors, ±SEM).

(B) Increased apoptosis by sustained MII inhibition. $CD34^+$-derived cells cultured in SCF and Tpo were treated with Blebb for 3 days and fixed, followed by intracellular flow cytometry with the anti-(cleaved caspase-3) and 7-AAD for DNA ($n = 3$, ±SEM, $p < 0.05$ for all except $CD34^-$ 4n).

(C) SR1 decreases the absolute number of apoptotic cells generated by Blebb treatment. Nucleated ($Hoechst^+$) Annexin-V^+ 7-AAD^- cells were quantified by flow cytometry calibrated by APC-beads. Absolute values were normalized to control (vehicle-treated cells). IC_{50} = ~380–1,200 nM, Hill coefficient = 0.62. *$p < 0.05$ Blebb +0 nM versus +750 nM SR1 ($n = 3$, ±SEM).

(D) Phenotypic HSC-enriched population is maximized by synergy between myosin inhibition and AHR antagonism. $CD34^+$-derived cells in SCF and Tpo were treated with different doses of the selective AHR antagonist SR1, with or without 20 μM Blebb for 3 days. Absolute values were normalized to 10^4 initial cell input and fit to dose-response curves. EC_{50} and maximum cell number for HSC-enriched, Control: 15.5 nM, 4000, and Blebb: 10 nM, 1800; MPP, Control: 15.5 nM, 2200, and Blebb: 15.5nM, 1,100; CPP, Control: 41.5 nM, 7,500, and Blebb: 4.7 nM, 2,400. Hill coefficient for all the graphs is ~1–2. $n \geq 3$ (±SEM).

(E) SR1 reverses upregulation of p53 protein by Blebb. Total p53 protein was quantified by intracellular flow cytometry. *ANOVA $p < 0.05$, Tukey's HSD Test $p < 0.05$ for DMSO versus Blebb ($n = 3$, ±SEM).

(F) Pharmacological inhibition of p53 transcription by cyclic-pifithrin-α increases the absolute cell number of phenotypic HSC-enriched. EC_{50} = 63.1 nM for both control and Blebb, Hill coefficient = 2.6, 1.8 for control and Blebb, respectively ($n = 3$, ±SEM).

(G) Summary of results for biological functions of MII in adult hematopoiesis with perturbations of MII pathways.

See also Figure S4, Figure S5, and Table S4.

key aspect of the MII isoform switch that defines and delineates hematopoiesis (Figure 7G).

How *MYH10* is ultimately repressed in differentiation requires further study: RUNX1 downregulates *MYH10* during MK differentiation (Lordier et al., 2012), but RUNX1 does not anticorrelate in general with *MYH10* and is not required for normal functions once HSCs are formed from vascular endothelial cells during embryonic development (Chen et al., 2009). Nevertheless, asymmetric processes are hinted at by a number of polarizable proteins in our early $CD34^+$ cells, including Cdc42, which polarizes in correlation with HSC aging (Florian et al., 2012). Generic polarization of a protein in hematopoietic cells seems predictive of a role in asymmetric division (Beckmann et al., 2007), but MIIB's role in physically breaking the symmetry of cytokinesis seems unique and motivates deeper study of biophysical factors that feed back into transcription programs and perhaps even regulate cancer stem cell differentiation (Cicalese et al., 2009).

Human HSC/Ps expand when cultured on flexible tropoelastin matrices plus serum and cytokines (Holst et al., 2010) and also expand when cultured serum-free on endothelial cells that secrete cytokines (Butler et al., 2012). However, endothelial cells and secreted matrix on plastic could be locally soft or regionally rigid. On FN-coated hydrogels that are marrow-mimetic soft or else endosteal-like stiff, minimal cytokines in serum-free media can for some conditions enrich for early $CD34^+$ cells, consistent with our finding that both soft gels and blebbistatin suppress MIIB polarization and enhance pS1943-MIIA in early $CD34^+$ cells.

Blood Cells that Lack Myosin-II Become Polyploid or Die Trying

Motile cells that are sufficiently adherent can generate enough traction forces to pull themselves apart even in the absence of MII, whereas cells in suspension or daughter cells that cannot

crawl away with sufficient force (to break the intercellular bridge) tend to become polyploid (Zang et al., 1997). HSC/Ps grow well as suspension cells that do not adhere and spread strongly on substrates compared to other solid tissue cell types, and they only possess a thin cortical cytoskeleton; cytokinesis defects are thus likely to favor polyploidy in these cell types. In a blood cancer line that only expresses MIIA, partial knockdown of MIIA indeed increases polyploidy in vitro as does blebbistatin and the cancer cells survive (Shin et al., 2011). In healthy human and mouse primary cells, however, such a process of endomitosis is usually seen only for MKs (among blood cells at least), which implies that other cell types are either never tetraploid or apoptose if they become so. Irreversible ablation in vivo of MIIA in primary blood cells indeed enhances apoptosis and depletes most dividing blood cell types (Figures 5D–5G). This seems consistent with cell death in blebbistatin treatments being downstream of MII inhibition. Although the specificity of this drug has been questioned (Shu et al., 2005), the reversible 3-day treatment here with blebbistatin of primary CD34+ cells in vitro increases ploidy of viable MKs and enhances apoptosis of progenitors with slower dividing stem/progenitor cells dying only with more sustained drug treatments. Our pharmacological results with AHR inhibitors provide some functional evidence of a transcriptome-implicated link between a failure of these normal primary, nonadherent cells to divide and AHR upstream of p53 in apoptosis (Figure 7G, right), but since AHR is primarily nuclear, any interaction with MII is likely to be indirect.

Translation

Mouse knockouts of MIIB are embryonic lethal (Ma et al., 2010), and since MIIA is at least weakly polarizable (Figure 2D), any deficiencies or mutations in MIIB might be partially compensated by MIIA. Inhibiting both isoforms transiently, as shown here, might be exploited to further maintain and perhaps expand HSCs and maybe other stem cells in suitably designed microenvironments. Importantly, given the successful long-term engraftment of drug treated cells, genes that are truly essential for hematopoiesis (profile in Figure 5Aii) might be clearly identified. Enrichment of highly adherent stem cells by the methods here might require optimization of adhesion to both suppress motility and provide sufficient anchorage signals for viability. Our findings ultimately reveal not only a biophysical hierarchy of actomyosin forces in adult hematopoiesis but also some utility in controlling those forces to enrich for stem cells.

EXPERIMENTAL PROCEDURES

MS-IF Cytometry

For intracellular flow cytometry, cells were fixed with 4% paraformaldehyde in PBS for 10 min, washed with PBS, and resuspended in 0.1% saponin in HBSS. The samples were then stained with antibodies against MIIA and MIIB for 30 min at room temperature, along with hematopoietic surface markers and Hoechst 33342, followed by secondary antibody staining conjugated with Alexa 488 and 647 (Invitrogen). The samples were analyzed on an LSR II (BD) to obtain the mean fluorescent intensity (MFI) values of MIIB and MIIA across different samples and subpopulations. Each value was normalized by a standard cell line (MFI from COS cells) to correct for differences in fluorescence intensities caused by laser fluctuations. Normalized MFI values from flow cytometry were then calibrated by MS results for MSCs (Raab et al., 2012) that served as a standard to calculate the stoichiometric ratio between MIIB and MIIA of each sample.

Standard methods can be found in Supplemental Experimental Procedures for MS, microarray, gene correlation analysis, cell culture, confocal microscopy, micropipette analysis, construction of matrix-coated gels, and xenotransplantation, among other techniques.

Statistical Analyses

All statistical analyses were performed using GraphPad Prism 5. Unless otherwise noted, all statistical comparisons were made by unpaired two-tailed Student t test and were considered significant if $p < 0.05$. All dose-response data were fitted to sigmoidal dose-response with variable slope with x axis in a log scale.

SUPPLEMENTAL INFORMATION

Supplemental Information for this article includes Supplemental Experimental Procedures, five figures, and five tables and can be found with this article online at http://dx.doi.org/10.1016/j.stem.2013.10.009.

AUTHOR CONTRIBUTIONS

J.W.S. and D.E.D. designed research; J.W.S., A.B., K.R.S., D.A.C., I.L.I., and F.R. performed research; J.S. and P.C.D. contributed to new analytic tools; C.L. and C.G. engineered, and C.A.H. supplied, the *MYH9* floxed mutant mice; and J.W.S., K.R.S., J.S., J.A.C., and D.E.D. wrote the paper.

ACKNOWLEDGMENTS

We thank Dr. Robert Adelstein, Dr. Mary Anne Conti (NIH-NHLBI), and Dr. Leonard Zon (Harvard) for invaluable comments. We gratefully acknowledge Arielle Glatman Zaretsky for technical assistance in mouse BM transplantation and the Stem Cell Xenograft Core at the University of Pennsylvania, A. Secreto, J. Glover, and Dr. G. Danet-Desnoyers for cells and engraftment studies. This study was supported by the National Institutes of Health (P01DK032094; R01HL062352; R01-EB007049; P30-DK090969; NCATS-8UL1TR000003), the Human Frontier Science Program (I.I. and D.E.D.), the National Science Foundation (D.E.D.), the Nano Science and Engineering Center-Nano Bio Interface Center (D.E.D.), and the American Heart Association (J.-W.S.).

Received: July 29, 2012
Revised: July 31, 2013
Accepted: October 17, 2013
Published: November 21, 2013

REFERENCES

Basu, S., Hodgson, G., Katz, M., and Dunn, A.R. (2002). Evaluation of role of G-CSF in the production, survival, and release of neutrophils from bone marrow into circulation. Blood *100*, 854–861.

Beckmann, J., Scheitza, S., Wernet, P., Fischer, J.C., and Giebel, B. (2007). Asymmetric cell division within the human hematopoietic stem and progenitor cell compartment: identification of asymmetrically segregating proteins. Blood *109*, 5494–5501.

Boitano, A.E., Wang, J., Romeo, R., Bouchez, L.C., Parker, A.E., Sutton, S.E., Walker, J.R., Flaveny, C.A., Perdew, G.H., Denison, M.S., et al. (2010). Aryl hydrocarbon receptor antagonists promote the expansion of human hematopoietic stem cells. Science *329*, 1345–1348.

Butler, J.M., Gars, E.J., James, D.J., Nolan, D.J., Scandura, J.M., and Rafii, S. (2012). Development of a vascular niche platform for expansion of repopulating human cord blood stem and progenitor cells. Blood *120*, 1344–1347.

Canman, J.C., Cameron, L.A., Maddox, P.S., Straight, A., Tirnauer, J.S., Mitchison, T.J., Fang, G., Kapoor, T.M., and Salmon, E.D. (2003). Determining the position of the cell division plane. Nature *424*, 1074–1078.

Chen, M.J., Yokomizo, T., Zeigler, B.M., Dzierzak, E., and Speck, N.A. (2009). Runx1 is required for the endothelial to haematopoietic cell transition but not thereafter. Nature *457*, 887–891.

Chen, G., Hou, Z., Gulbranson, D.R., and Thomson, J.A. (2010). Actin-myosin contractility is responsible for the reduced viability of dissociated human embryonic stem cells. Cell Stem Cell *7*, 240–248.

Cicalese, A., Bonizzi, G., Pasi, C.E., Faretta, M., Ronzoni, S., Giulini, B., Brisken, C., Minucci, S., Di Fiore, P.P., and Pelicci, P.G. (2009). The tumor suppressor p53 regulates polarity of self-renewing divisions in mammary stem cells. Cell *138*, 1083–1095.

Clark, K., Langeslag, M., van Leeuwen, B., Ran, L., Ryazanov, A.G., Figdor, C.G., Moolenaar, W.H., Jalink, K., and van Leeuwen, F.N. (2006). TRPM7, a novel regulator of actomyosin contractility and cell adhesion. EMBO J. *25*, 290–301.

Conti, M.A., Even-Ram, S., Liu, C., Yamada, K.M., and Adelstein, R.S. (2004). Defects in cell adhesion and the visceral endoderm following ablation of nonmuscle myosin heavy chain II-A in mice. J. Biol. Chem. *279*, 41263–41266.

Doulatov, S., Notta, F., Laurenti, E., and Dick, J.E. (2012). Hematopoiesis: a human perspective. Cell Stem Cell *10*, 120–136.

Dulyaninova, N.G., House, R.P., Betapudi, V., and Bresnick, A.R. (2007). Myosin-IIA heavy-chain phosphorylation regulates the motility of MDA-MB-231 carcinoma cells. Mol. Biol. Cell *18*, 3144–3155.

Engler, A.J., Sen, S., Sweeney, H.L., and Discher, D.E. (2006). Matrix elasticity directs stem cell lineage specification. Cell *126*, 677–689.

Florian, M.C., Dörr, K., Niebel, A., Daria, D., Schrezenmeier, H., Rojewski, M., Filippi, M.D., Hasenberg, A., Gunzer, M., Scharffetter-Kochanek, K., et al. (2012). Cdc42 activity regulates hematopoietic stem cell aging and rejuvenation. Cell Stem Cell *10*, 520–530.

Fuentes, R., Wang, Y., Hirsch, J., Wang, C., Rauova, L., Worthen, G.S., Kowalska, M.A., and Poncz, M. (2010). Infusion of mature megakaryocytes into mice yields functional platelets. J. Clin. Invest. *120*, 3917–3922.

Fulcher, D.A., and Basten, A. (1997). B cell life span: a review. Immunol. Cell Biol. *75*, 446–455.

Giebel, B., Corbeil, D., Beckmann, J., Höhn, J., Freund, D., Giesen, K., Fischer, J., Kögler, G., and Wernet, P. (2004). Segregation of lipid raft markers including CD133 in polarized human hematopoietic stem and progenitor cells. Blood *104*, 2332–2338.

Hawkins, E.D., Hommel, M., Turner, M.L., Battye, F.L., Markham, J.F., and Hodgkin, P.D. (2007). Measuring lymphocyte proliferation, survival and differentiation using CFSE time-series data. Nat. Protoc. *2*, 2057–2067.

Holst, J., Watson, S., Lord, M.S., Eamegdool, S.S., Bax, D.V., Nivison-Smith, L.B., Kondyurin, A., Ma, L., Oberhauser, A.F., Weiss, A.S., and Rasko, J.E. (2010). Substrate elasticity provides mechanical signals for the expansion of hemopoietic stem and progenitor cells. Nat. Biotechnol. *28*, 1123–1128.

Kiel, M.J., Yilmaz, O.H., Iwashita, T., Yilmaz, O.H., Terhorst, C., and Morrison, S.J. (2005). SLAM family receptors distinguish hematopoietic stem and progenitor cells and reveal endothelial niches for stem cells. Cell *121*, 1109–1121.

Knoblich, J.A. (2010). Asymmetric cell division: recent developments and their implications for tumour biology. Nat. Rev. Mol. Cell Biol. *11*, 849–860.

Kovács, M., Tóth, J., Hetényi, C., Málnási-Csizmadia, A., and Sellers, J.R. (2004). Mechanism of blebbistatin inhibition of myosin II. J. Biol. Chem. *279*, 35557–35563.

Lichtman, M.A. (1970). Cellular deformability during maturation of the myeloblast. Possible role in marrow egress. N. Engl. J. Med. *283*, 943–948.

Lordier, L., Bluteau, D., Jalil, A., Legrand, C., Pan, J., Rameau, P., Jouni, D., Bluteau, O., Mercher, T., Leon, C., et al. (2012). RUNX1-induced silencing of non-muscle myosin heavy chain IIB contributes to megakaryocyte polyploidization. Nat Commun *3*, 717.

Ma, X., Jana, S.S., Conti, M.A., Kawamoto, S., Claycomb, W.C., and Adelstein, R.S. (2010). Ablation of nonmuscle myosin II-B and II-C reveals a role for nonmuscle myosin II in cardiac myocyte karyokinesis. Mol. Biol. Cell *21*, 3952–3962.

Majeti, R., Park, C.Y., and Weissman, I.L. (2007). Identification of a hierarchy of multipotent hematopoietic progenitors in human cord blood. Cell Stem Cell *1*, 635–645.

Maupin, P., Phillips, C.L., Adelstein, R.S., and Pollard, T.D. (1994). Differential localization of myosin-II isozymes in human cultured cells and blood cells. J. Cell Sci. *107*, 3077–3090.

Merkel, R., Simson, R., Simson, D.A., Hohenadl, M., Boulbitch, A., Wallraff, E., and Sackmann, E. (2000). A micromechanic study of cell polarity and plasma membrane cell body coupling in Dictyostelium. Biophys. J. *79*, 707–719.

Nilsson, S.K., Debatis, M.E., Dooner, M.S., Madri, J.A., Quesenberry, P.J., and Becker, P.S. (1998). Immunofluorescence characterization of key extracellular matrix proteins in murine bone marrow in situ. J. Histochem. Cytochem. *46*, 371–377.

Nishino, T., Wang, C., Mochizuki-Kashio, M., Osawa, M., Nakauchi, H., and Iwama, A. (2011). Ex vivo expansion of human hematopoietic stem cells by garcinol, a potent inhibitor of histone acetyltransferase. PLoS ONE *6*, e24298.

Notta, F., Doulatov, S., Laurenti, E., Poeppl, A., Jurisica, I., and Dick, J.E. (2011). Isolation of single human hematopoietic stem cells capable of long-term multilineage engraftment. Science *333*, 218–221.

Novershtern, N., Subramanian, A., Lawton, L.N., Mak, R.H., Haining, W.N., McConkey, M.E., Habib, N., Yosef, N., Chang, C.Y., Shay, T., et al. (2011). Densely interconnected transcriptional circuits control cell states in human hematopoiesis. Cell *144*, 296–309.

Oguro, H., Ding, L., and Morrison, S.J. (2013). SLAM family markers resolve functionally distinct subpopulations of hematopoietic stem cells and multipotent progenitors. Cell Stem Cell *13*, 102–116.

Ou, G., Stuurman, N., D'Ambrosio, M., and Vale, R.D. (2010). Polarized myosin produces unequal-size daughters during asymmetric cell division. Science *330*, 677–680.

Pietrancosta, N., Maina, F., Dono, R., Moumen, A., Garino, C., Laras, Y., Burlet, S., Quéléver, G., and Kraus, J.L. (2005). Novel cyclized Pifithrin-alpha p53 inactivators: synthesis and biological studies. Bioorg. Med. Chem. Lett. *15*, 1561–1564.

Raab, M., Swift, J., Dingal, P.C., Shah, P., Shin, J.W., and Discher, D.E. (2012). Crawling from soft to stiff matrix polarizes the cytoskeleton and phosphoregulates myosin-II heavy chain. J. Cell Biol. *199*, 669–683.

Ren, Y., Effler, J.C., Norstrom, M., Luo, T., Firtel, R.A., Iglesias, P.A., Rock, R.S., and Robinson, D.N. (2009). Mechanosensing through cooperative interactions between myosin II and the actin crosslinker cortexillin I. Curr. Biol. *19*, 1421–1428.

Rodriguez, P.L., Harada, T., Christian, D.A., Pantano, D.A., Tsai, R.K., and Discher, D.E. (2013). Minimal "Self" peptides that inhibit phagocytic clearance and enhance delivery of nanoparticles. Science *339*, 971–975.

Sedzinski, J., Biro, M., Oswald, A., Tinevez, J.Y., Salbreux, G., and Paluch, E. (2011). Polar actomyosin contractility destabilizes the position of the cytokinetic furrow. Nature *476*, 462–466.

Shin, J.-W., Swift, J., Spinler, K.R., and Discher, D.E. (2011). Myosin-II inhibition and soft 2D matrix maximize multi-nucleation and cellular projections typical of platelet-producing megakaryocytes. Proc. Nat. Acad. Sci. USA *108*, 11458–11463.

Shu, S., Liu, X., and Korn, E.D. (2005). Blebbistatin and blebbistatin-inactivated myosin II inhibit myosin II-independent processes in Dictyostelium. Proc. Natl. Acad. Sci. USA *102*, 1472–1477.

Sneddon, I.N. (1965). The relation between load and penetration in the axisymmetric boussinesq problem for a punch of arbitary profile. Int. J. Eng. Sci. *3*, 47–57.

Sprent, J., and Basten, A. (1973). Circulating T and B lymphocytes of the mouse. II. Lifespan. Cell. Immunol. *7*, 40–59.

Takenaka, K., Prasolava, T.K., Wang, J.C., Mortin-Toth, S.M., Khalouei, S., Gan, O.I., Dick, J.E., and Danska, J.S. (2007). Polymorphism in Sirpa modulates engraftment of human hematopoietic stem cells. Nat. Immunol. *8*, 1313–1323.

Ting, S.B., Deneault, E., Hope, K., Cellot, S., Chagraoui, J., Mayotte, N., Dorn, J.F., Laverdure, J.P., Harvey, M., Hawkins, E.D., et al. (2012). Asymmetric segregation and self-renewal of hematopoietic stem and progenitor cells with endocytic Ap2a2. Blood *119*, 2510–2522.

Trumpp, A., Essers, M., and Wilson, A. (2010). Awakening dormant haematopoietic stem cells. Nat. Rev. Immunol. *10*, 201–209.

Ubukawa, K., Guo, Y.M., Takahashi, M., Hirokawa, M., Michishita, Y., Nara, M., Tagawa, H., Takahashi, N., Komatsuda, A., Nunomura, W., et al. (2012). Enucleation of human erythroblasts involves non-muscle myosin IIB. Blood *119*, 1036–1044.

van Furth, R., and Cohn, Z.A. (1968). The origin and kinetics of mononuclear phagocytes. J. Exp. Med. *128*, 415–435.

Vaziri, C., and Faller, D.V. (1997). A benzo[a]pyrene-induced cell cycle checkpoint resulting in p53-independent G1 arrest in 3T3 fibroblasts. J. Biol. Chem. *272*, 2762–2769.

Vicente-Manzanares, M., Koach, M.A., Whitmore, L., Lamers, M.L., and Horwitz, A.F. (2008). Segregation and activation of myosin IIB creates a rear in migrating cells. J. Cell Biol. *183*, 543–554.

Wang, F., Kovacs, M., Hu, A., Limouze, J., Harvey, E.V., and Sellers, J.R. (2003). Kinetic mechanism of non-muscle myosin IIB: functional adaptations for tension generation and maintenance. J. Biol. Chem. *278*, 27439–27448.

Yamazaki, S., Ema, H., Karlsson, G., Yamaguchi, T., Miyoshi, H., Shioda, S., Taketo, M.M., Karlsson, S., Iwama, A., and Nakauchi, H. (2011). Nonmyelinating Schwann cells maintain hematopoietic stem cell hibernation in the bone marrow niche. Cell *147*, 1146–1158.

Zang, J.H., Cavet, G., Sabry, J.H., Wagner, P., Moores, S.L., and Spudich, J.A. (1997). On the role of myosin-II in cytokinesis: division of Dictyostelium cells under adhesive and nonadhesive conditions. Mol. Biol. Cell *8*, 2617–2629.

Zuco, V., and Zunino, F. (2008). Cyclic pifithrin-alpha sensitizes wild type p53 tumor cells to antimicrotubule agent-induced apoptosis. Neoplasia *10*, 587–596.

Cell Stem Cell, volume *14*

Supplemental Information

Contractile Forces Sustain and Polarize Hematopoiesis from Stem and Progenitor Cells

Jae-Won Shin, Amnon Buxboim, Kyle R. Spinler, Joe Swift, David A. Christian, Christopher A. Hunter, Catherine Léon, Christian Gachet, P.C. Dave P. Dingal, Irena L. Ivanovska, Florian Rehfeldt, Joel Anne Chasis, and Dennis E. Discher

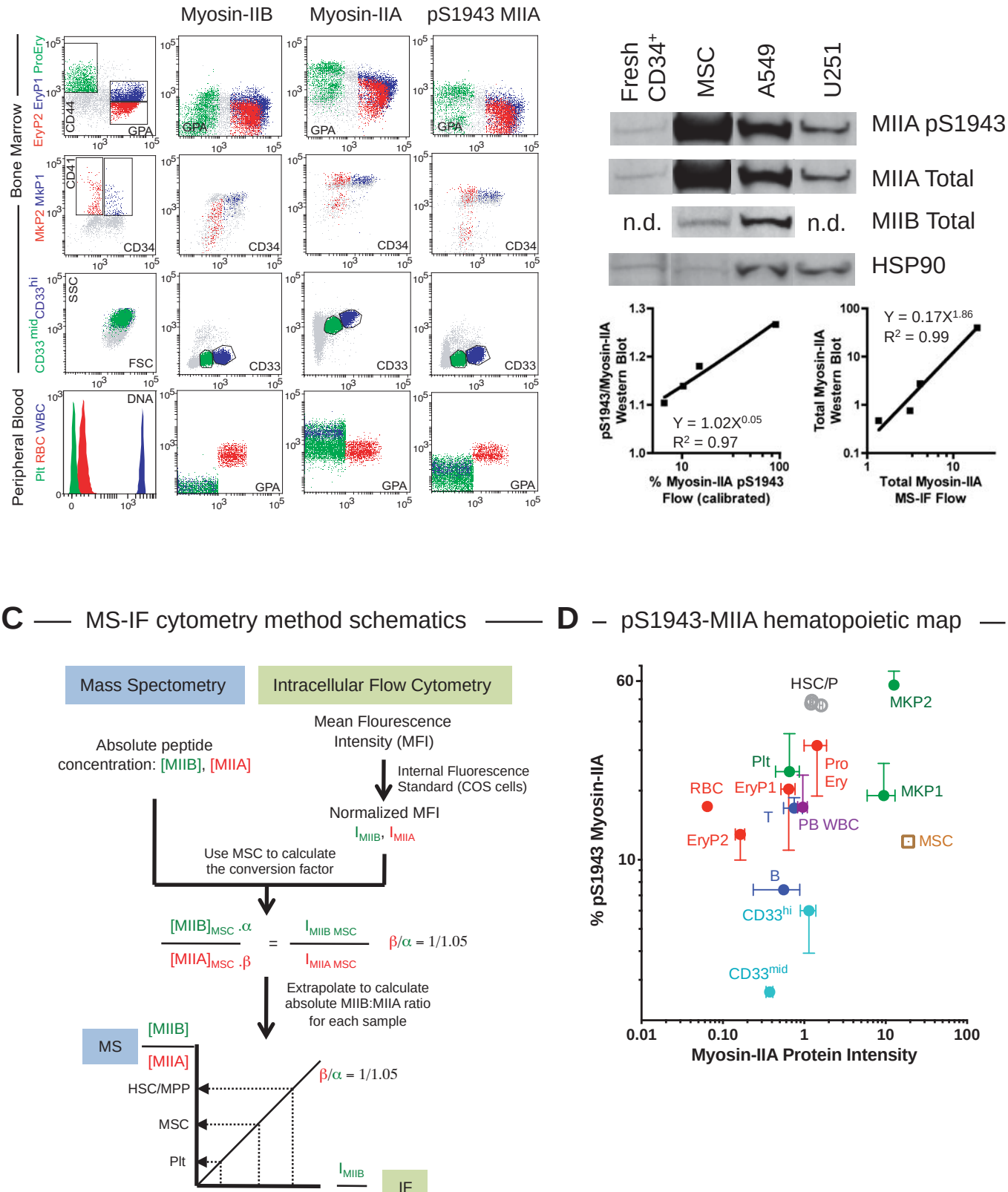
A
Intracellular flow cytometry
Myosin-IIB
Myosin-IIA
pS1943 MIIA
Bone Marrow
Peripheral Blood
EryP2 EryP1 ProEry
MkP2 MkP1
CD33mid CD33hi
Plt RBC WBC
CD44
CD41
SSC
FSC
DNA
GPA
CD34
CD33
B
Western blot validation
Fresh CD34+
MSC
A549
U251
MIIA pS1943
MIIA Total
MIIB Total
HSP90
n.d.
pS1943/Myosin-IIA Western Blot
% Myosin-IIA pS1943 Flow (calibrated)
Y = 1.02X0.05
R2 = 0.97
Total Myosin-IIA Western Blot
Total Myosin-IIA MS-IF Flow
Y = 0.17X1.86
R2 = 0.99
C
MS-IF cytometry method schematics
Mass Spectometry
Intracellular Flow Cytometry
Absolute peptide concentration: [MIIB], [MIIA]
Mean Flourescence Intensity (MFI)
Internal Fluorescence Standard (COS cells)
Normalized MFI
IMIIB, IMIIA
Use MSC to calculate the conversion factor
[MIIB]MSC .α / [MIIA]MSC .β = IMIIB MSC / IMIIA MSC
β/α = 1/1.05
Extrapolate to calculate absolute MIIB:MIIA ratio for each sample
MS
[MIIB]
[MIIA]
HSC/MPP
MSC
Plt
β/α = 1/1.05
Plt
MSC
HSC MPP
IMIIB / IMIIA
IF
D
pS1943-MIIA hematopoietic map
% pS1943 Myosin-IIA
Myosin-IIA Protein Intensity
HSC/P
MKP2
Plt
Pro Ery
RBC
EryP1
MKP1
T
PB WBC
EryP2
MSC
B
CD33hi
CD33mid

Fig. S1

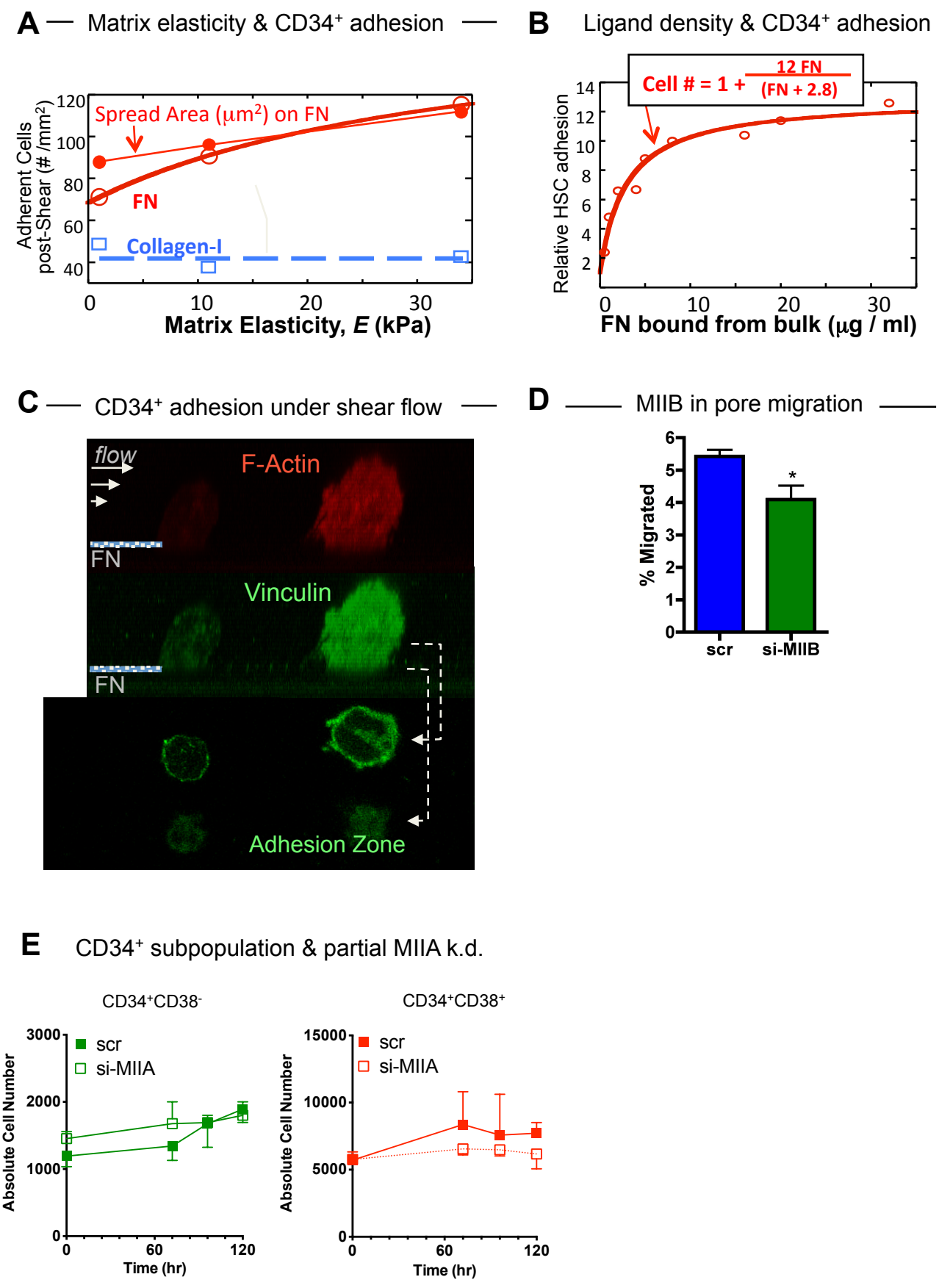
A
Matrix elasticity & CD34+ adhesion
Adherent Cells post-Shear (# /mm2)
Spread Area (μm2) on FN
FN
Collagen-I
Matrix Elasticity, E (kPa)
B
Ligand density & CD34+ adhesion
Cell # = 1 + 12 FN / (FN + 2.8)
Relative HSC adhesion
FN bound from bulk (μg / ml)
C
CD34+ adhesion under shear flow
flow
F-Actin
FN
Vinculin
FN
Adhesion Zone
D
MIIB in pore migration
% Migrated
scr
si-MIIB
E
CD34+ subpopulation & partial MIIA k.d.
CD34+CD38-
CD34+CD38+
scr
si-MIIA
Absolute Cell Number
Time (hr)

Fig. S2

A hCD47⁺hCD45⁺ cells in NSG

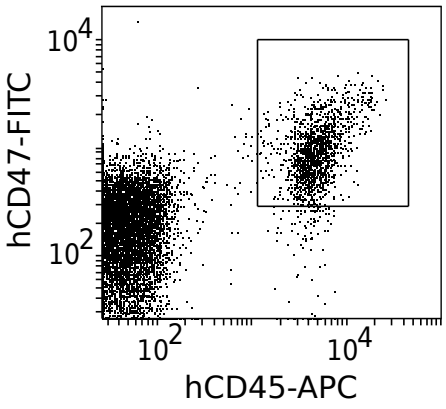

B Primary and secondary human LT-HSC engraftment

Samples	CD34+ after culture	Primary Transplant	Secondary Transplant
Untreated	67,267	5/8	1/5
	119,485	8/10	2/4
	295,767	8/8	3/4
Blebbistatin	13,791	4/8	0/5
	20,290	8/10	3/5
	47,856	7/8	4/6

Samples	Primary SRC frequency per initial injected CD34+ cell	95% Confidence Interval	P-value
Untreated	1/68,883	1/40,079-1/118,388	
Blebbistatin	1/17,511	1/10,455-1/29,330	P<0.0005

Samples	Secondary SRC frequency per initial injected CD34+ cell	95% Confidence Interval	P-value
Untreated	1/214,849	1/93,542-1/493,467	
Blebbistatin	1/44,615	1/20,929-1/95,108	P<0.01

C Human RBCs in NSG mice

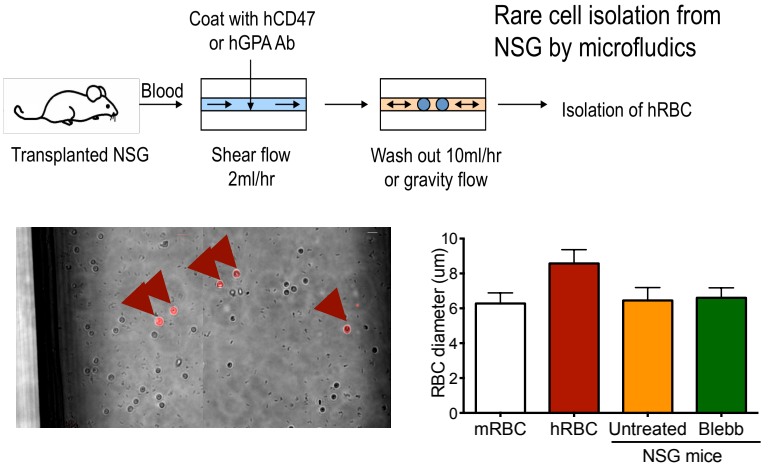

D Human CD34⁺ cells in NSG

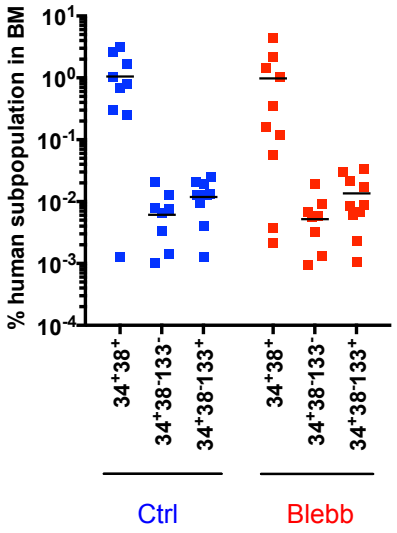

E Human MK decay kinetics

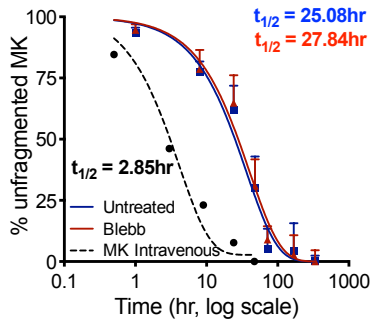

F Human plt size in NSG

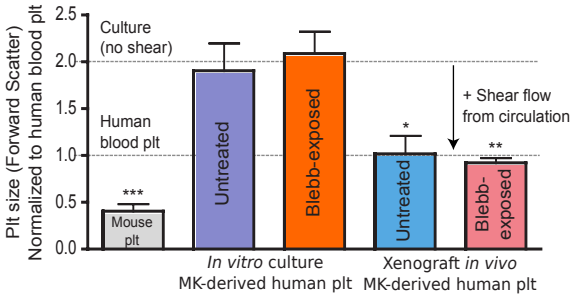

G Blebb & progenitors

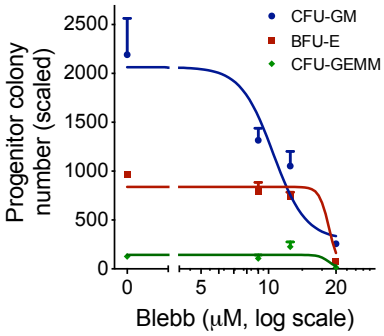

Fig. S3

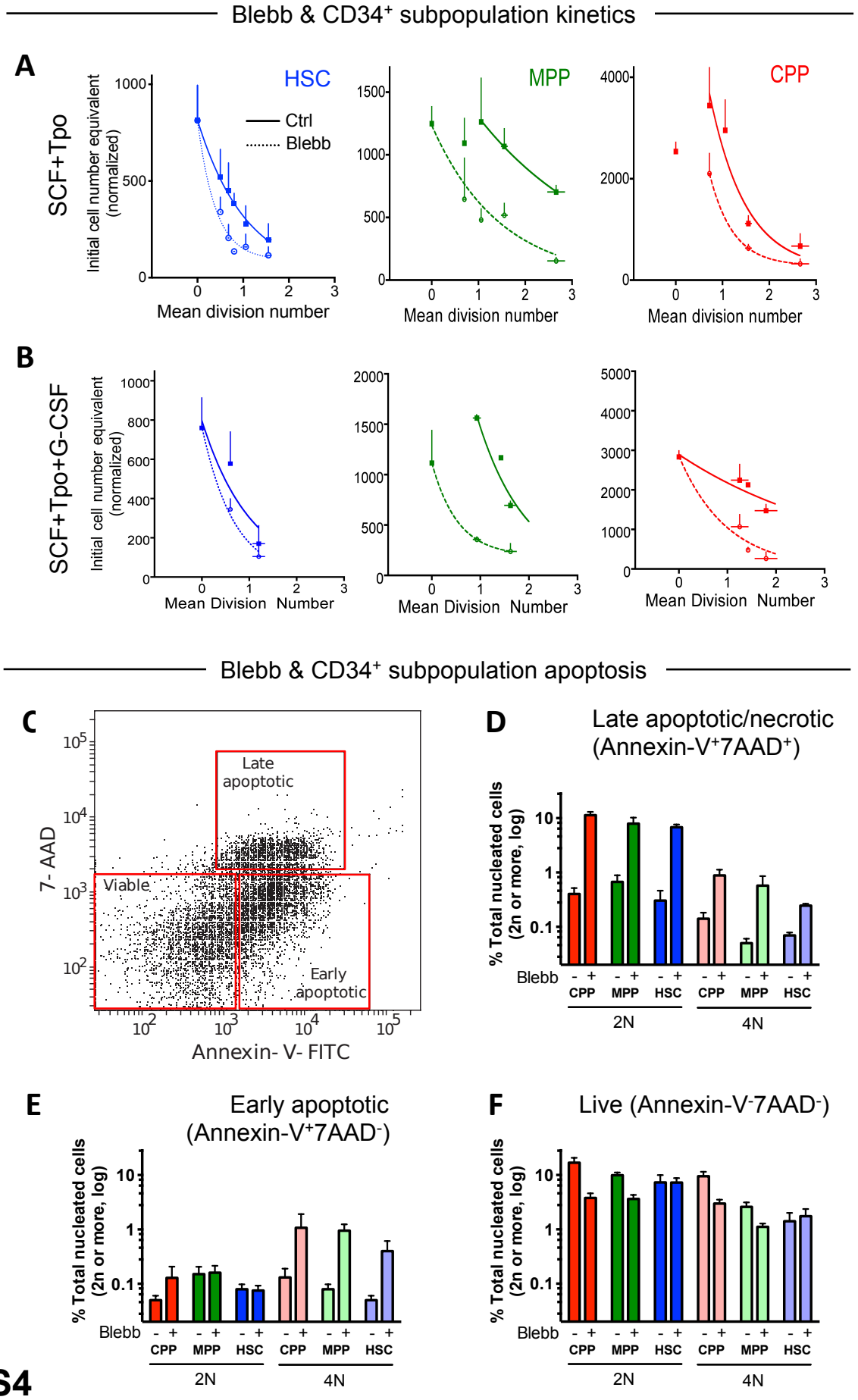
Blebb & CD34⁺ subpopulation kinetics
A
SCF+Tpo
Initial cell number equivalent (normalized)
HSC
MPP
CPP
Ctrl
Blebb
Mean division number
B
SCF+Tpo+G-CSF
Mean Division Number
Blebb & CD34⁺ subpopulation apoptosis
C
7- AAD
Annexin- V- FITC
Late apoptotic
Viable
Early apoptotic
D
Late apoptotic/necrotic (Annexin-V⁺7AAD⁺)
% Total nucleated cells (2n or more, log)
Blebb
CPP MPP HSC CPP MPP HSC
2N
4N
E
Early apoptotic (Annexin-V⁺7AAD⁻)
F
Live (Annexin-V⁻7AAD⁻)

Fig. S4

A

Dose-response fit of AHR antagonists & CD34⁺ cell number

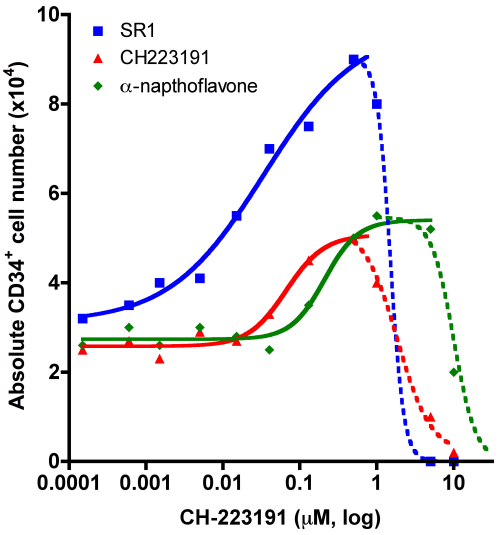

B

Effects of CH-223191 and Blebb on CD34⁺ subpopulations

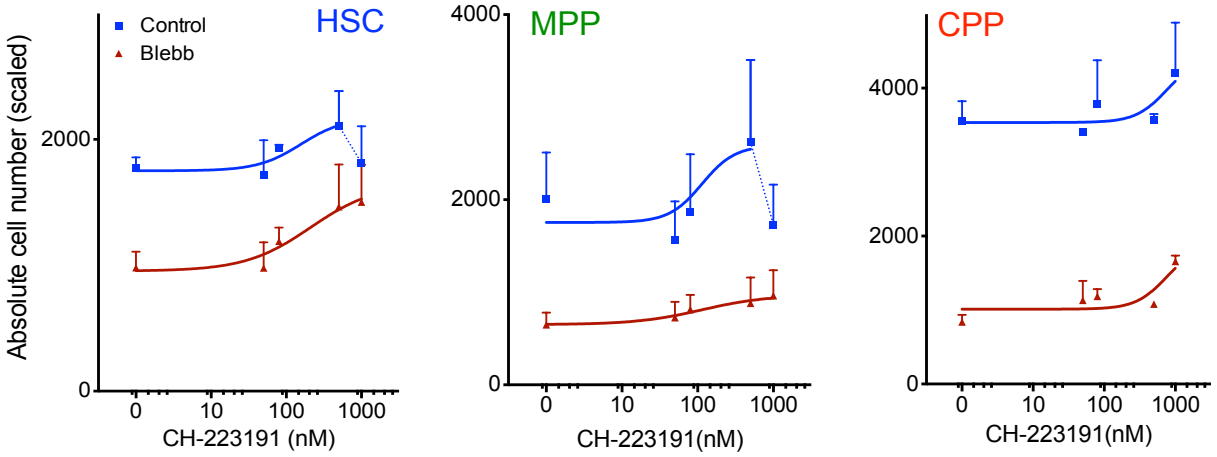

Fig. S5

Cell Type	MIIB	MIIA	B:A	B+A
MSC	1.2630	18.8856	0.0638*	20.0911
"HSC"	0.4141 ± 0.0092	1.2391 ± 0.0448	0.3204 ± 0.0149	1.6344 ± 0.0433
"MPP"	0.3051 ± 0.0058	1.2150 ± 0.0444	0.2407 ± 0.0104	1.5062 ± 0.0435
"CPP"	0.1511 ± 0.0025	1.3567 ± 0.1883	0.0782 ± 0.0234	1.7350 ± 0.0475
CD33mid	0.0070 ± 0.0070	0.3754 ± 0.0362	0.0163 ± 0.0163	0.3821 ± 0.0429
CD33hi	0.0412 ± 0.0117	1.1415 ± 0.2456	0.0334 ± 0.0027	1.1808 ± 0.2566
$CD3^+$ (T)	0.0032 ± 0.0012	0.7526 ± 0.1963	0.0054 ± 0.0019	0.7556 ± 0.1954
$CD19^+$ (B)	0.0004 ± 0.0004	0.5576 ± 0.3215	0.0016 ± 0.0016	0.5580 ± 0.3211
ProE	0.2771 ± 0.1351	1.4362 ± 0.4405	0.1502 ± 0.0518	1.7006 ± 0.5560
EryP1	0.0962 ± 0.0408	0.6442 ± 0.1273	0.1357 ± 0.0562	0.7360 ± 0.1562
EryP2	0.0231 ± 0.0088	0.1636 ± 0.0214	0.1585 ± 0.0740	0.1857 ± 0.0195
RBC	0.0414	0.5196	0.1827	0.0763
MKP2	0.8736	12.6413	0.0660	13.4751
MKP1	1.9188 ± 0.0268	9.4722 ± 3.5470	0.2237 ± 0.0811	11.3036 ± 3.5726
Plt	0.0011 ± 0.0011	0.6558 ± 0.2126	0.0023 ± 0.0023	0.6568 ± 0.2116
WBC	0.0077 ± 0.0077	0.9580 ± 0.1305	0.0089 ± 0.0089	0.8422 ± 0.1231
*:Mass spectrometry measurement				

Table S1

Supplemental Figure and Table Legends

Figure S1. (*Related to Figure 1*) **(A)** Representative intracellular FACS dot plots show lineage subpopulations (1st column) and expression of MIIA, pS1943 and MIIB (Y-axis) across lineages (markers indicated in X-axis) (2nd-4th column). **(B)** Validation of flow cytometry results by Western blotting. (Top) Representative bands corresponding to each of MIIA pS1943, MIIA, MIIB (250kD) and HSP90 (90kD) are shown. (Bottom) Intensity data from Western blot were plotted against the corresponding MS-IF data. Data were fitted to a power-law graph ($Y = A.X^B$). **(C)** Schematics of MS-IF-cytometry. Detailed description is available in Supplemental Experimental Procedures. **(D) %** pS1943-MIIA versus total MIIA map similar to Fig. 1A (n ≥ 3 donors, ± SEM).

Figure S2. (*Related to Figure 2 and 3*) **(A)** The number of adherent cells after shear (per mm^2) on FN or collagen-I-coated gels with different elasticity. **(B)** Effects of FN concentrations on cell adhesion (relative number of cells adhered). **(C)** Confocal imaging of cells adhered on fibronectin followed by shear flow. Cells were stained with phalloidin (F-actin, red) and vinculin (green). **(D)** MIIB knockdown partially impairs migration of HSC/MPP phenotypic cells through 3μm pore. *P<0.05, scrambled vs MIIB siRNA, n=4 donors (± SEM). **(E)** $CD34^+$ cell numbers do not change after partial MIIA knockdown (30%), evaluated by CFSE tracking as in Fig. 3E (n = 2 donors, ± SEM).

Figure S3. (*Related to Figure 6)* **(A)** Representative plot showing that most $hCD45^+$ cells from BM are $hCD47^+$ (~97%) in NSG mice 16-wk after transplantation of human $CD34^+$ cells. **(B)** (Top) Summary of primary and secondary NSG transplantation data. (Bottom) Estimation of human SRC frequency in NSG mice by extreme limiting dilution analysis (ELDA) (Hu and Smyth, 2009). **(C)** (Top) Rare human RBC isolation from NSG blood transplanted with human $CD34^+$-derived cells by a microfluidics channel adsorbed with anti-human CD47 antibody. (Bottom, left) Adhered human RBCs were visualized by staining with PE anti-human GPA (red). (Bottom, right) Average RBC diameter (in μm, n > 20 measurements for each group). **(D)** Quantification of human BM $CD34^+CD38^+$, $CD34^+CD38^-CD133^-$, and $CD34^+CD38^-CD133^+$ subpopulations from NSG mice xenografted with human $CD34^+$ cells, showing no difference between control and Blebb-exposed. **(E)** Calculation of MK decay rate. Integration of **Fig. 6C** reflects net production by MKs and, while dominated by Phase-II, it suggests a roughly first order process with MK half-life regardless of drug treatment of 25~28 hrs**;** this is ~10 times longer than the same analysis for intravenous infused MKs (Fuentes et al., 2010) and seems suggestive of intrabone transplantation (n=10 recipients ± SEM). **(F)** Human-$CD41^+$ platelets derived in vivo after transplantation into NSC mice show the normal platelet size compared to human blood platelets. ANOVA P<0.0001. *P<0.05 for untreated *in vitro* vs *in vivo*. **P<0.01 for Blebb-exposed *in vitro* vs *in vivo*. ***P<0.001 for untreated *in vivo* vs mouse plt. n = 5 per sample (± SEM). **(G)** Colony forming assays demonstrate reduced progenitor numbers by myosin inhibition. CFU-GM IC50 = ~10.5 μM, Hill coefficient = -6; BFU-E IC50 = 18.6 μM, Hill coefficient = -20 (n ≥ 3 donors, ± SEM). Note that BFU-E and CFU-GEMM numbers are not

changed under ~15 μM, while CFU-GM number is significantly reduced.

Figure S4. (*Related to Figure 7*) **(A)** Kinetics of HSC/P division indicates accelerated cell decay with Blebb (20 μM). Cells were cultured with SCF and Tpo. Half-life values respectively for Control and Blebb: HSC = 0.72 and 0.28; MPP = 1.88 from division 1 and 1.01; CPP = 0.53 and 0.35 from division 0.7 (n ≥ 3 donors, ± SEM). **(B)** G-CSF enhances protection of HSCs but accelerates progenitor decay under blebbistatin treatment (n ≥ 3 donors, ± SEM). Half-life values: HSC untreated = 0.71; HSC blebb = 0.47; MPP untreated = 0.69 from division 1; MPP blebb = 0.37; CPP untreated = 2.44; HSC blebb = 0.69. Microarray profiling above shows as expected that the G-CSF receptor (*CSF3R*) is a low intensity gene that is 2-3-fold upregulated upon differentiation toward $CD34^-$ cells (Table S4). **(C-F)** Flow cytometric analysis of apoptosis after blebbistatin treatment by Annexin-V (aV) and 7AAD. **(C)** Representative flow cytometry plot showing late apoptotic/necrotic (aV^+7AAD^+), early apoptotic (aV^+7AAD^-), live (aV^-7AAD^-) populations of cells treated with 20 μM blebbistatin. Percentages of total nucleated cells for 2n and 4n compartments (nuclear content analyzed by Hoechst 33342) are indicated as bar graphs for **(D)** late apoptotic/necrotic **(E)** early apoptotic and **(F)** live populations (n = 3 donors, ± SEM).

Figure S5. (*Related to Figure 7*) **(A)** The dose-response effect of AHR inhibitors on $CD34^+$ cell number. Data are derived from Boitano et al. (2010) and fitted with a dose-response curve. SR1 (blue): EC50 = 47.4 nM, Hillslope = 0.64; CH-223191 (red): EC50 = 74 nM, Hill slope = 1.6; a-napthoflavone (green): EC50 = 177nM, Hillslope = 2.0. Drugs show toxic effect at 500 nM or above for SR1 and CH-223191, while 1uM or above for a-napthoflavone. **(B)** HSC number is maximized by synergy between myosin inhibition and the selective AHR antagonist CH-223191, with or without 20 μM Blebb for 3 d in SCF and Tpo. Absolute values were normalized to 10^4 initial cell input and fit to dose-response curves. (EC50, Maximum cell number) for:,HSC (Control: 158 nM, 2100) and (Blebb: 211 nM, 1800); MPP (Control: 114 nM, 2200) and (Blebb: 114 nM, 1000); CPP (Control: 750 nM, 4100) and (Blebb: 750 nM, 1500). n = 3 donors, ± SEM.

Table S1. *(Related to Figure 1)* MIIB and MIIA protein expression values calibrated by MS-IF.

Table S2. *(Related to Figure 1)* The list of correlated genes with *MYH10* based on the "robust to analysis" criteria.

Table S3. *(Related to Figure 3)* Gene correlation list of candidate genes involved in asymmetric division and polarization.

Table S4. *(Related to Figure 4, 6, 7)* Expression profiles of selected genes relevant to signaling of myosin-IIA heavy chain phosphorylation, hematopoietic lineage differentiation, and apoptosis. NT: Non-Treated; TR: Blebb-Treated.

Table S5. *(Related to Figure 6)* List of genes showing selective expression in functional long-term multilineage reconstituting cells-enriched $CD34^+$ cells by blebbistatin in comparison to fresh HSC/P subpopulations (fold changes in $\log_2$).

Supplemental Experimental Procedures

Cell culture. Fresh purified bone marrow-derived human $CD34^+$ cells were obtained from either the Penn Xenograft Core Facility or AllCells (Emeryville, CA). Cells from at least 20 different donors were used in this study. Purity of the samples (>98 %) was confirmed by flow cytometry with monoclonal antibody against human CD34. All experiments were performed in HSC expansion media (StemLine, Sigma) supplemented with 1x antibiotics, 20% BIT 9500 Serum Substitute (StemCell Technologies), 2 mM L-glutamate (Gibco) and the following human recombinant cytokines: stem cell factor (SCF, 100 ng/ml) and thrombopoietin (Tpo, 100 ng/ml). In some occasions, the media was also supplemented by granulocyte-colony stimulating factor (G-CSF, 100 ng/ml), epidermal growth factor (EGF, 100 ng/ml), transforming growth factor beta 1 (TGF-beta1, 100 ng/ml), erythropoietin (EPO, 1 U/ml) and interleukin-3 (IL-3, 10 ng/ml). All cytokines were purchased from R&D Systems. After cells were cultured for 4 days, they were treated with different doses of cellular contractility inhibitors, including (±)-blebbistatin (EMD Biosciences) and/or CH-223191 (Sigma) and StemRegenin-1 (Cellagen Technology, San Diego, CA) for indicated durations of up to 3 days. Cells were cultured at 37°C in 5% CO2.

Antibody staining and flow cytometry. Surface marker analysis for HSC/Ps was done on either a LSR II flow cytometer or FACSCalibur (Becton Dickinson). Fresh or cultured $CD34^+$-derived cells were stained in staining media (2% FBS in PBS) at room temperature for 1 h with PE or APCCy7 anti-CD34 (581, Invitrogen or Biolegend), PECy7 anti-CD38 (HIT2, eBioscience), PECy5.5 anti-CD45RA (MEM-56, Invitrogen), APC anti-CD90 (5E10, BD Bioscience), washed and stained with Hoechst 33342 (Invitrogen) at 37°C for 30min to stain nuclei, followed by washing with staining media with 7-AAD (Sigma) to exclude dead cells. Cells isolated from the bone marrow stained for 1 h with APC anti-mouse CD47 (miap301, AbD Serotec), FITC anti-human CD47 (BD Biosciences), and PE anti-human CD11b, PE anti-human CD19 (both from BD Biosciences), or PE anti-human Glycophorin A (Invitrogen). Platelets and RBCs were analyzed by staining with PE anti-mouse CD41 (eBioscience) and FITC anti-human CD41 (eBioscience) for 20min, followed by analysis on FACSCalibur on log forward and side scatter scales.

Intracellular flow cytometry. The method was modified from a protocol described previously (Gibbs et al., 2011) for HSC/Ps. Cells were fixed with 4% paraformaldehyde in PBS for 10 min, washed with PBS and resuspended in 0.1% saponin in HBSS (staining medium). The samples were then stained with antibodies against cytoplasmic antigens, including MIIA (Sigma), MIIB, phospho-MIIA, pan-p53, and caspase-3 (all from Cell Signaling Technology) for 30 min at room temperature. In some cases, cells were concurrently stained with PE anti-CD34 or anti-human CD38 for subpopulation analysis. Cells were then washed and stained with anti-rabbit or mouse secondary antibodies conjugated with Alexa 647 (Invitrogen) for 30 min, followed by analysis on FACSCalibur.

CFSE labeling. $CD34^+$-derived cells were labeled with CFSE (2.5 μM) in PBS/5% FBS for 3 min

in dark at room temperature and washed once with PBS/5% FBS and once with HSC expansion media. The labeled cells were analyzed every day for 3 days using multi-color flow cytometry with HSC/P markers. Given that cell division is unsynchronized, cell numbers from different CFSE peaks are normalized by dividing the cell numbers by $2^{\text{division number}}$ to correct for the effect of cell expansion. The mean division number from each sample was calculated by fitting normalized CFSE data to the normal distribution curve and taking its mean value. The cell decay rate was calculated as described previously (Gett and Hodgkin, 2000): Each peak represents a cohort of cells that entered their first division at the same time, and so one can calculate how many cells of each type underwent each division with the decay in cell number versus division number reflecting proliferation, differentiation, and cell death.

DNA Microarray Transcriptional Profiling and Gene Expression Correlation Analysis. Total RNA was extracted from cells using Trizol and isolated by RNeasy (Qiagen) according to manufacturer's protocol. Total RNA was amplified and converted to cDNA using WT-Ovation Pico kit (NuGen) and converted to ST-cDNA, fragmented and biotin-functionalized using WT-Ovation Exon Mudule (NuGen). Hybridization cocktails were prepared at 45.4, 15.1 and 7.6 ng/µl ST-cDNA and mixed with Eukaryotic Hybridization Controls (GeneChip) at proportional concentrations. Each Sample was interrogated by sequential hybridization, rinse and scan cycles on a single Human Gene 1.0 ST DNA microarray (Affymetrix), from low to high concentration, and followed by two rinse-scan cycles in which no sample was added. In each experiment the scanned intensities that were obtained from all samples, five scans per array, were mutually RMA-summarized to transcription clusters gene levels so that the average and standard deviation values (STD) could be calculated for each gene ("Titrated-RMA"). In addition, raw intensities as a function of relative sample concentration were fitted by standard binding curves so that non-saturating and background-subtracted levels were evaluated ("SPEC method", Detailed description is available in Buxboim et al., 2012). Average gene-expression levels ± STD of fresh HSC, MPP and CPP, and cultured $CD34^+$ and $CD34^-$ treated or untreated with blebbistatin samples were evaluated by averaging across five array scans. Values from each sample were averaged from two biologically independent experiments. Color-coded gene symbols represent the *absolute* gene expression levels of the biologically replicated averages of across samples. Pearson Correlation (MeV) was used to perform correlation analyses of the entire genome against *MYH10*, as well as to cluster samples and genes. Dendograms (Fig. 6A, ii) represent the correlative proximity of log-base-2 gene expression fold changes.

Cell culture and transfection in COS-1 cells. COS-1 cells were obtained from ATCC (Manassas, VA) and were maintained in high glucose DMEM with 10% FBS. Lipofectamene 2000 was used for both siRNA knockdown of MIIB and overexpression of MIIA constructs, according to the manufacturer's instruction (Invitrogen), when cells were 5-10% and 60-70% confluent, respectively. Efficiency of MIIB siRNA was confirmed to be >90% as indicated by quantitative immunofluorescence analysis. For GFP-tagged MIIA constructs, the transfection efficiency was about 30~40%. Cells were then subjected to micropipette aspiration or replated on FN-coated gels to study cell spreading.

Electroporation of nucleic acid in cell culture. Primary $CD34^+$ cell culture and MEG01 cell line were transfected with DNA constructs or MIIB siRNA by electroporation ("nucleofection") using the Nucleofector kits (**Lonza**) as described in the manual. Briefly, cultured cells were washed with PBS and resuspended with transfection solution containing 2μg/ml DNA constructs or 3μg/ml siRNA. They were then transferred into a cuvette and transfected with the Nucleofector II. The medium at 37°C was then added to transfected cells. Cells were incubated overnight and then the medium was exchanged to fresh on the next day. The siRNA sequences used for MIIB and MIIB knockdown are described previously (Raab et al., 2012; Shin et al., 2011).

Western Blotting. Cells were washed with ice-cold PBS and lysed on ice with lysis buffer (150 mM sodium chloride, 1% Nonidet P-40, 1% protease inhibitor mixture 50mM Tris at pH 8.0) mixed with 1x NuPage LDS sample buffer (Invitrogen) for 30 min with sonication. Samples were then boiled for 10min at 90~100^{0}C, followed by centrifugation for 5min at 10,000rpm. For Western blot, whole lysate were separated on 3% to 7% Tris-Acetate gels (NuPAGE, Invitrogen). The proteins were then transferred to a polyvinylidene fluoride (PVDF) membrane with an iBlot Gel Transfer Device (Invitrogen), followed by blocking with 5% nonfat dry milk solution for 1 h. Incubation with primary antibodies was done at 4 °C overnight with 1:1,000 total MIIA (Sigma), MIIB or pS1943 (Cell Signaling Technology. After washing, the membrane was incubated with 1:2,500 anti-rabbit and 1:1,000 anti-mouse HRP-conjugated IgG antibodies at room temperature for 1 h. The blot was developed with ChromoSensor (GenScript) for 5 min, followed by digital scanning to perform densitometry analysis by ImageJ (National Institutes of Health).

Micropipette aspiration. Fresh BM $CD34^+$ cells or transfected COS-1 cells in suspension were subjected to micropipette analysis. Capillary tubes of 1.0 mm inner diameter (World Precision Instruments, Sarasota, FL) were pulled into micropipettes using a Flaming-Brown Micropipette Puller (Sutter Instrument, Novato, CA) and cut further using a deFonbrune-type microforge (Vibratome, St. Louis, MO). The average micropipette diameter was around 3 μm. Micropipettes were attached to a dual-stage water manometer with reservoirs of adjustable height. Suction was applied by a syringe, and the corresponding pressure was measured by pressure transducer (Validyne, Northridge, CA) calibrated by a mercury U-tube manometer. Pressures for different experiments ranged from 0.5 to 15 kPa.

Construction of FN-coated gels with different matrix elasticity. 15~18mm glass coverslips were treated in order with ethanol, RCA solution (1:1:3 for 15N NH_4OH:30% H_2O_2:dH_2O), methylene chloride and 0.1% allyltrichlorosilane solution. To control gel's stiffness, n,n′methylene-bis-acrylamide and the acrylamide solution was mixed at the ratio of 0.07%:3% for soft gels (0.3kPa), or the ratio of 0.3%:8% for stiff gels (34kPa), final concentrations in PBS. ~25 μl of the mixed solution was polymerized on a coverslip with 10% ammonium persulfate and n,n,n′,n′-tetramethylethylenediamine. During polymerization, gels were covered with

another coverslip to obtain a uniform gel surface with the final thickness of ~100 μm. Different concentrations of FN were then cross-linked with polymerized gels using sulfo-SANFAH (Pierce, Rockford, IL) by UV-crosslinking. Thickness of gels and relative FN concentrations were verified by confocal microscopy – we assume that most FN from the solution was attached to gels (>70%). FN-coated gels were then treated with UV in PBS for at least 1hr before use in cell culture.

Immunofluorescence analysis. Cells on coverslips were fixed with 4% paraformaldehyde, followed by permeabilization with 0.5% Triton X-100 in PBS for 15min and blocking with 1% BSA in PBS for 30min. Samples were then stained with primary antibodies (1:100 for all antibodies used) overnight at 4C. After washing, staining with appropriate Alexa 488 or 647-conjugated secondary antibodies (1:400) and TRITC-phalloidin was performed for 45min at room temperature. Cells were washed three times with PBS and mounted in ProLong Gold antifade medium (Invitrogen). Samples were then analyzed by fluorescence microscopy.

Dual immunofluorescence staining of MII isoforms. Fixed and permeabilized cells were stained first with either rabbit anti-MIIB or anti-pS1943 MIIA, followed by Alexa 488-conjugated secondary antibody for 1 hr at room temperature. The samples were then fixed with 4% paraformaldehyde for 5min. Meanwhile, anti-MIIA was conjugated with Alexa 647 using the Zenon Rabbit IgG labeling kit (Invitrogen) as described in the manual. The fixed samples were then incubated with Alexa 647-conjugated anti-MIIA for 30 min. The samples were fixed again with 4% paraformaldehyde for 5min, washed with PBS 3 times, and mounted in the antifade medium for fluorescence microscopy.

Cell sorting. BM $CD34^+$-derived cells at d7 were stained with CD41-FITC at room temperature for 1hr, followed by with Annexin-V-PE (BD Biosciences) in the Annexin-V staining medium for 15min. Cells were then resuspended in 2% FBS/PBS with 7-AAD. Viable HSC/Ps and differentiated cells at day 7 culture were separated on the basis of CD34 surface expression by cell sorting performed on a FACS Vantage™ machine (Becton Dickinson). Dead cells stained with 7-Amino-actinomycin D (7-AAD) and Annexin-V were excluded from sorting. Sorted cells were directly processed for microarray analysis.

Colony forming assay. 1000-3000 $CD34^+$-derived cells were seeded into methylcellulose containing media (MethoCult H4434, StemCell Technologies) supplemented with SCF, GM-CSF, IL-3, Epo. They were cultured for day 14 and colonies were scored at 10x magnification based on the published morphological criteria by StemCell Technoloigies. Colony forming content was normalized per 10,000 cells seeded.

Engraftment of $CD34^+$ cells in NSG mice and limiting dilution analysis. BM-derived $CD34^+$ cells were cultured in SCF and Tpo (100 ng/ml each) for 4 days and treated under control conditions or blebbistatin (20 μM) for 3 days. The cells were injected intra-tibially into sub-lethally irradiated (250 rads) 6-10-week-old NSG mice within 24 h after irradiation. Engraftment

was assessed by analysis of blood or bone marrow using anti-mouse and anti-human CD47 antibodies using flow cytometry. The mice were sacrificed after 16 weeks post-transplantation. For secondary engraftment, 50% of the bone marrow from femurs and tibias from each mouse was transplanted into one sub-lethally irradiated NSG mouse. 16 weeks after transplantation, blood and bone marrow were harvested from the mice and analyzed by flow cytometry. All animal experiments were done in accordance with institutional guidelines approved by the ethical committee from the University of Pennsylvania. The human repopulation HSC frequency was quantified by extreme limiting dilution analysis (ELDA) software (Hu and Smyth, 2009).

Lentiviral transduction of CD34$^+$ cells. For MIIB knockdown experiment, fresh human BM CD34$^+$ cells were transduced with lentiviral vector containing MIIB shRNA sequence previously verified (pLKO.1-puro, Sigma):
5'-CCGGGCCAACATTGAAACATACCTTCTCGAGAAGGTATGTTTCAATGTTGGCTTTTTG-3'
Transduction was done on plate coated with 100ng/ml retronectin (Lonza) in the presence of 5μg/ml polybrene (Sigma). After 2d transduction, untransduced cells were selected by adding 1μg/ml puromycin for 2d, followed by transplantation.

Inducible knockout mice, transplantation and engraftment. Cre;MYH9$^{loxP/loxP}$ mice were produced by the laboratory of Catherine Léon and Christian Gachet (Université de Strasbourg) and provided by the laboratory of Christopher Hunter (University of Pennsylvania). 8-12 week-old gender-matched mice were used. For competitive repopulation, a total of 2 million donor BM cells from Cre;MYH9$^{loxP/loxP}$ (CD45.2) and genetically matched WT mice (CD45.1) were mixed 1:1 and injected retro-orbitally into the lethally irradiated recipient WT mice (B6.SJL, CD45.1$^+$). 8 weeks later, 20mg/ml tamoxifen in sterilized corn oil (both from Sigma) was administered into the recipient mice 5 times for one week to induce *MYH9* deletion. Chimerism was determined by flow cytometry analysis on PB at indicated time points, and the mice were sacrificed after 8 wks of *MYH9* deletion to perform BM and SP analysis.

Rare human blood cell isolation from NSG mice. The surface of micro-channel slide (μ-Slide VI, Ibidi) was coated with anti-human CD47 antibody via adsorption overnight at 4^{o}C. The coated chamber was then blocked with 1% BSA/PBS for 30min before use. Approximately, 500 μl of blood cells derived from NSG mice transplanted with human cells were diluted in PBS/1% BSA and passed through the antibody-coated chamber using a syringe pump (~10 ml/hr), followed by washout with PBS/1% BSA for 10 min. Human RBCs remaining on the chamber were subjected to immunofluorescence with anti-human GPA antibody staining. The experimental samples were compared to the control sample derived from uninjected NSG mice.

Mass spectrometry calibrated intracellular flow cytometry (MS-IF-cytometry). The conversion scheme is described in **Fig. S1C**. After intracellular flow cytometry to obtain the mean fluorescent intensity (MFI) values of MIIB and MIIA across different samples, each value was normalized by the internal fluorescence standard (MFI value from COS cells) to correct for differences in fluorescence intensities caused by laser fluctuations from a flow cytometer. After

this, the normalized MFI values from flow cytometry were calibrated against mass spectrometry results based on the following:

From flow cytometry:

$$[B]_{\mathrm{MSC}} \cdot \alpha = I^{B}_{\mathrm{MSC}}$$

$$[A]_{\mathrm{MSC}} \cdot \beta = I^{A}_{\mathrm{MSC}}$$

Where [B] and [A] represent concentrations of myosin-II B and A, a and b are instrument response functions (in this case, direct proportionality) and *I* is the mean fluorescence intensity in either myosin-II channel from flow cytometry. From mass spectrometry, the absolute ratio between isoforms is defined as R.

$$\frac{[B]_{\mathrm{MSC}}}{[A]_{\mathrm{MSC}}} = R_{\mathrm{MSC}}$$

The estimate of R_{MSC} is 6:94. Combine instrument response functions into k, which can be defined from experimentally measureable terms (using MSC as a standard):

$$\frac{\alpha}{\beta} = \frac{I^{B}_{\mathrm{MSC}}}{I^{A}_{\mathrm{MSC}} \cdot R_{\mathrm{MSC}}} = k$$

k = 1.05. Other samples can then be characterized from flow cytometry measurements, based on calibration through this scaling factor:

$$\frac{[B]_x}{[A]_x} = \frac{I^{B}_{x}}{I^{A}_{x} \cdot k}$$

$$[B]_x + [A]_x = \frac{I^{B}_{x}}{\alpha} + \frac{I^{A}_{x}}{\beta} = \beta^{-1} \cdot \left(\frac{I^{B}_{x}}{k} + I^{A}_{x} \right)$$

$$[B]_x + [A]_x \propto \left(\frac{I^{B}_{x}}{k} + I^{A}_{x} \right)$$

Evaluation of the percentage of MIIA pS1943 from intracellular flow cytometry results. Mean fluorescence intensity of MIIA pS1943 and total MIIA MSCs was evaluated by intracellular flow cytometry along with other cell types. MIIA pS1943 content in MSCs was quantified by

immuno-depletion of pS1943 using the phospho-specific antibody: Immuno-depleted vs pS1943-enriched fractions were separated by immunoprecipitation and western blotting was done to quantify the relative ratio of total MIIA between two fractions. % MIIA pS1943 values in MSCs range from 10 to 20% and the average value (12%) was used to calibrate the values from all the samples.

Supplemental References

Fuentes, R., Wang, Y., Hirsch, J., Wang, C., Rauova, L., Worthen, G.S., Kowalska, M.A., and Poncz, M. (2010). Infusion of mature megakaryocytes into mice yields functional platelets. J Clin Invest *120*, 3917-3922.

Gett, A.V., and Hodgkin, P.D. (2000). A cellular calculus for signal integration by T cells. Nat Immunol *1*, 239-244.

Gibbs, K.D., Jr., Gilbert, P.M., Sachs, K., Zhao, F., Blau, H.M., Weissman, I.L., Nolan, G.P., and Majeti, R. (2011). Single-cell phospho-specific flow cytometric analysis demonstrates biochemical and functional heterogeneity in human hematopoietic stem and progenitor compartments. Blood *117*, 4226-4233.

Hu, Y., and Smyth, G.K. (2009). ELDA: extreme limiting dilution analysis for comparing depleted and enriched populations in stem cell and other assays. J Immunol Methods *347*, 70-78.

Raab, M., Swift, J., Dingal, P.C., Shah, P., Shin, J.W., and Discher, D.E. (2012). Crawling from soft to stiff matrix polarizes the cytoskeleton and phosphoregulates myosin-II heavy chain. J Cell Biol *199*, 669-683.

Shin, J.W., Swift, J., Spinler, K.R., and Discher, D.E. (2011). Myosin-II inhibition and soft 2D matrix maximize multinucleation and cellular projections typical of platelet-producing megakaryocytes. Proc Natl Acad Sci U S A *108*, 11458-11463.